Measurement of Cosmic Ray Proton + Helium Flux with the DAMPE Experiment

PhD thesis defense
Gran Sasso Science Institute
23/04/2020

Candidate : Zhaomin Wang

Supervisor : Prof. Ivan De Mitri

CONTENTS

PART 01

Introduction

Introduction

- **Cosmic Ray (CR) overview**
- **Recent CR observations below the “knee”**
- **Motivation of the thesis**

Cosmic Ray (CR) overview

In 1912, Victor Hess measured the ionization rate up to the height of 5200 m, pointing out the existence of CR;

In 1927, Jacob Clay found a variation of the CR intensity with the latitude;

In 1939, Pierre Auger and his collaborators found that groups of particles could simultaneously reach detectors that were separated as large as 200 m;

In 1941, Marcel Schein found that CRs are mainly protons;

In 1962, John Linsley observed an CR event with energy of 10^{20} eV;

….

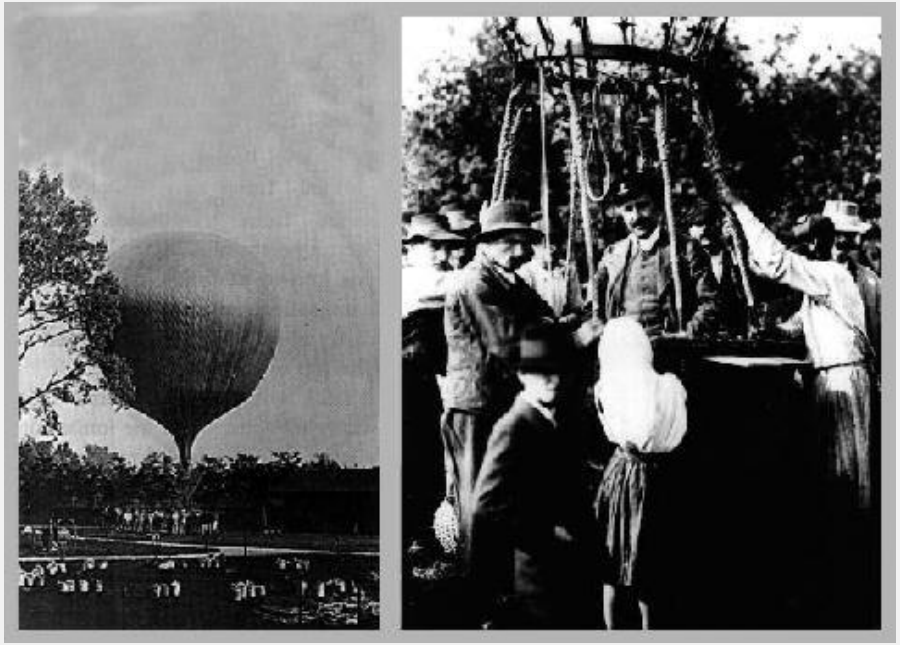

Cosmic Ray (CR) overview

Early CR observations revealed that the feature of CR spectrum follows approximatively a single power law until the so-called “knee” region (~ 3 PeV). Then again till the so-called “ankle” region(~ 3 EeV) and the highest energies.

In 1949, Enrico Fermi proposed a CR acceleration mechanism (Second order of Fermi mechanism), which leads to a power law spectrum feature.

In the 1970s, researchers proposed a more efficient mechanism (Diffusive shock mechanism or First order mechanism), in which the spectral index can be derived quantitatively and can explain experimental data.

However…

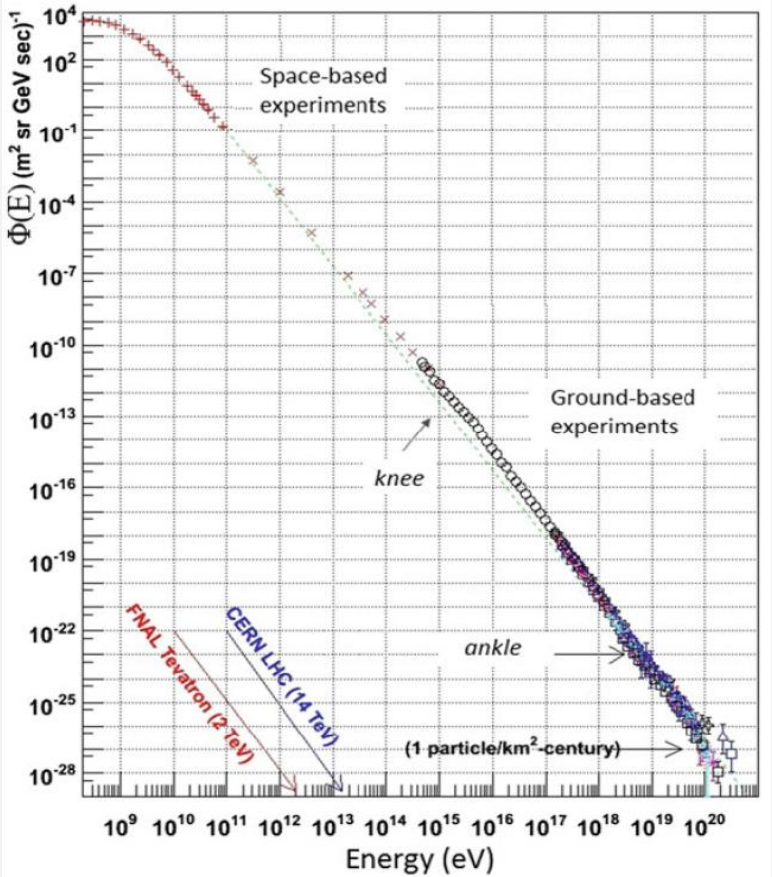

Introduction

- Cosmic Ray (CR) overview
- Recent CR observations below the “knee”
- Motivation of the thesis

Recent CR observations below the "knee"

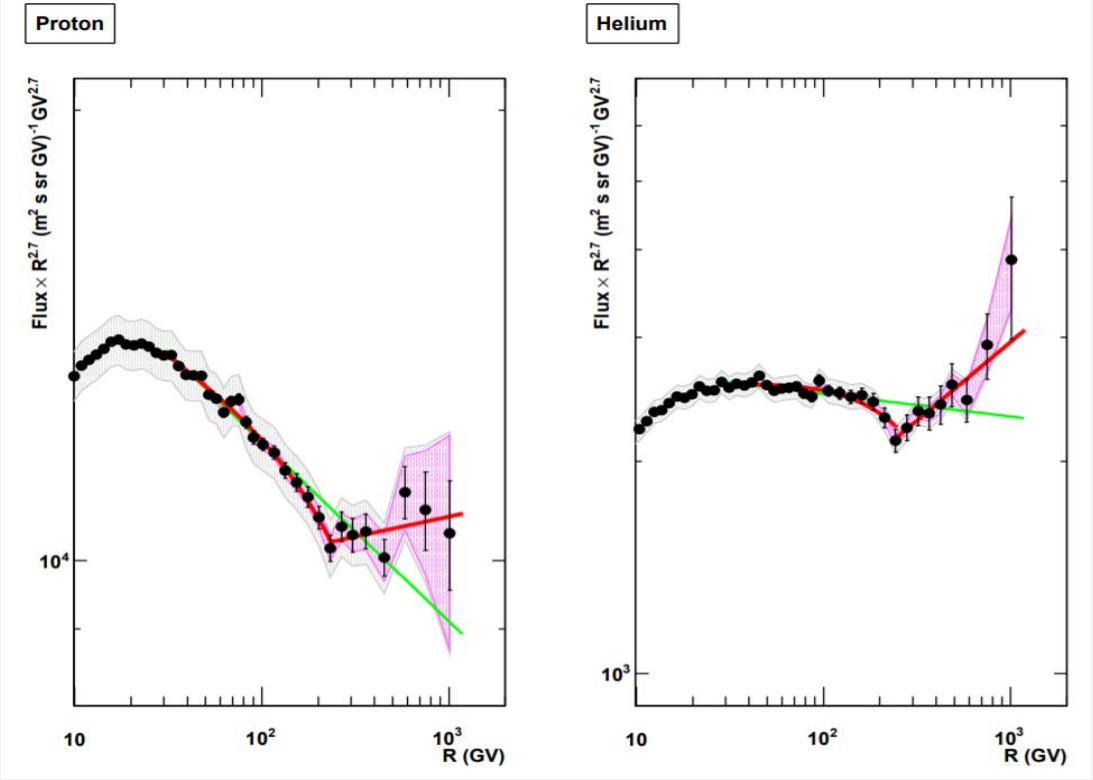

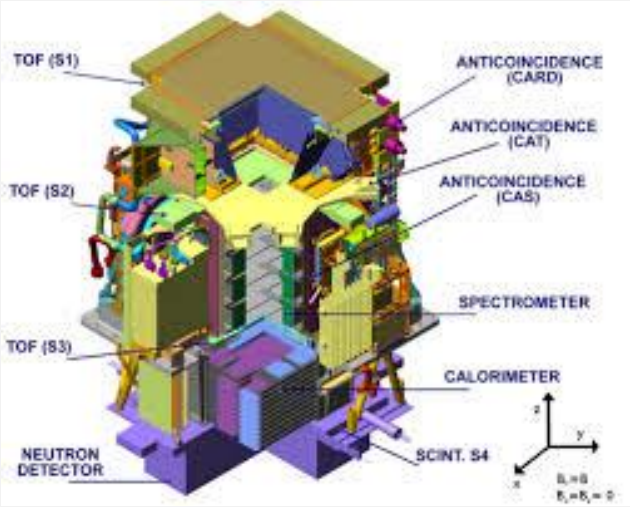

A spectral hardening at ~240 GV is found for both proton and helium spectra.

Introduction

Recent CR observations below the "knee"

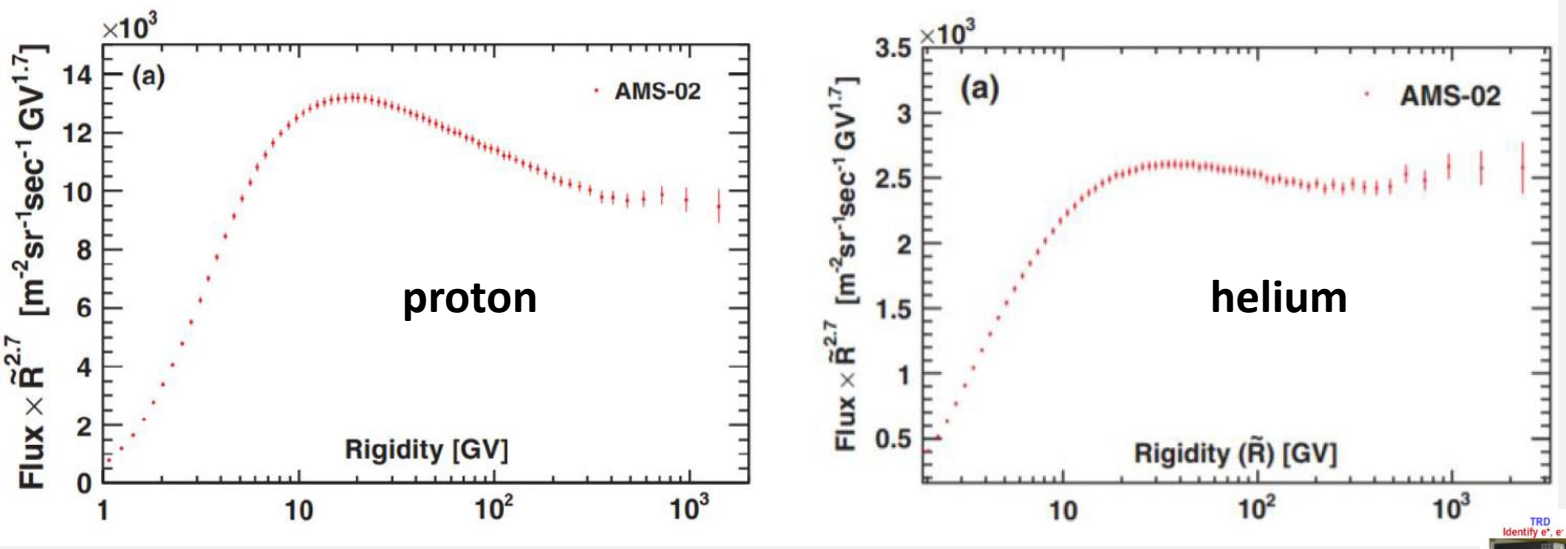

AMS-02 confirmed, with better precision, the PAMELA observations: the spectral hardenings are found at ~330 GV for proton and ~240 GV for helium.

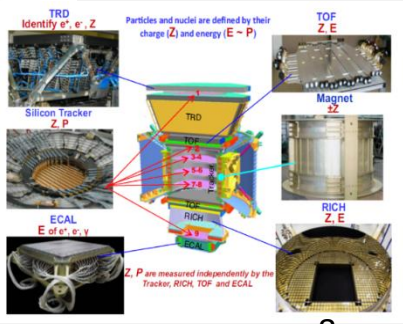

Recent CR observations below the "knee"

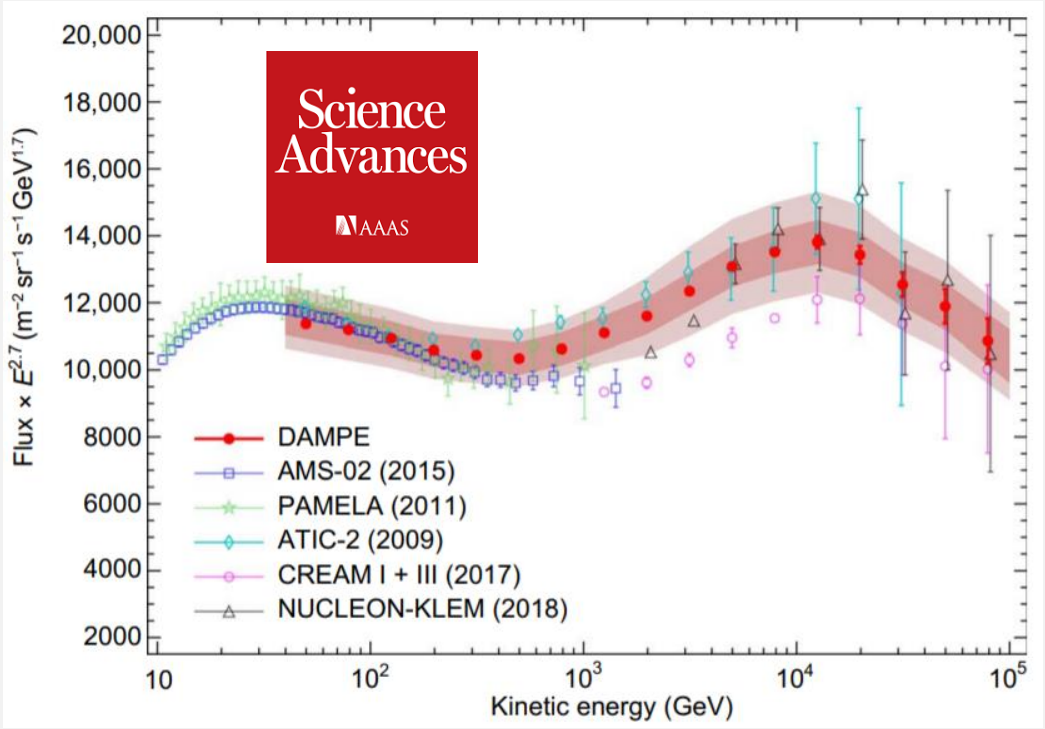

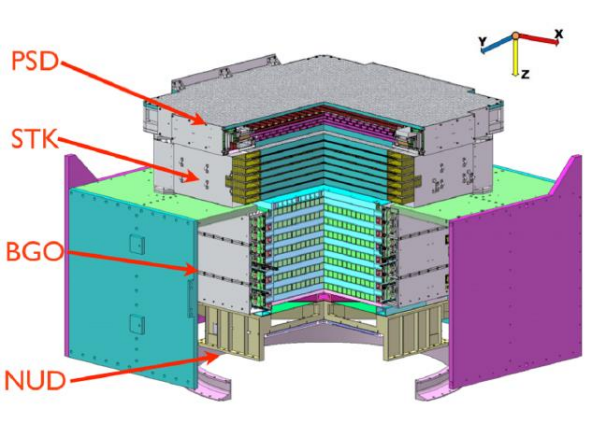

The recent published proton spectrum from DAMPE confirms the spectral hardening at ~300 GeV found by the previous experiments and reveals a softening at ~13.6 TeV with significance of 4.7 σ.

Introduction

- Cosmic Ray (CR) overview
- Recent CR observations below the “knee”
- **Motivation of the thesis**

Motivation of the thesis

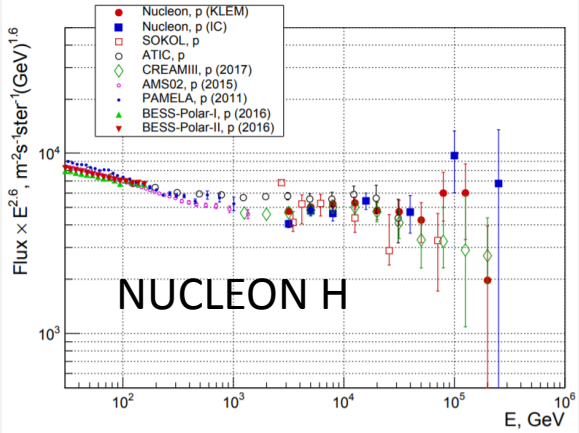

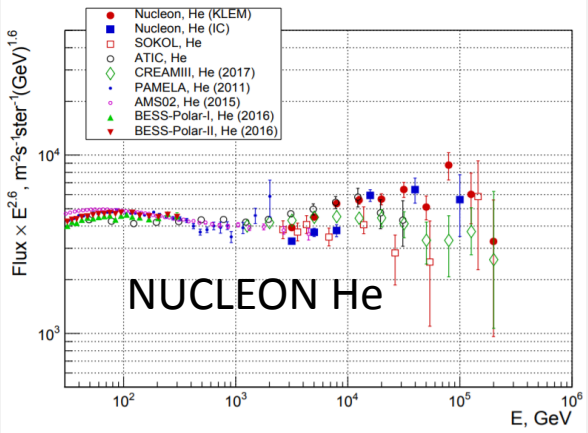

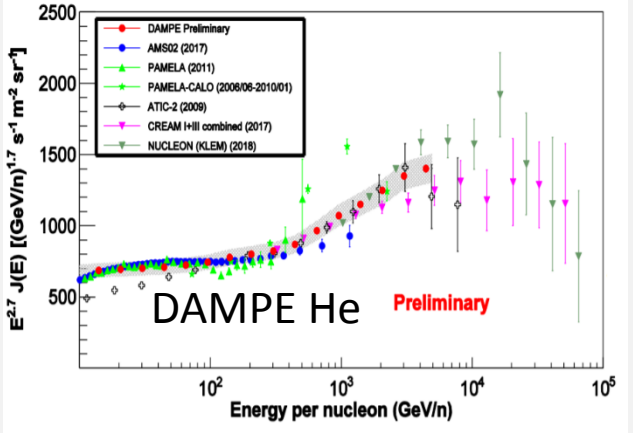

More observations on CR nuclei spectrum with energy range between 1 TeV up to 100 TeV are needed.

Motivation of the thesis

- Measuring the H + He can enhance our understanding on CR nuclei spectral features with energy below 100 TeV
- Selecting the H + He samples has the advantages of almost no background and very high purity
- Going towards higher energies, a comparison on the light nuclei spectrum between the direct and indirect measurements can be done

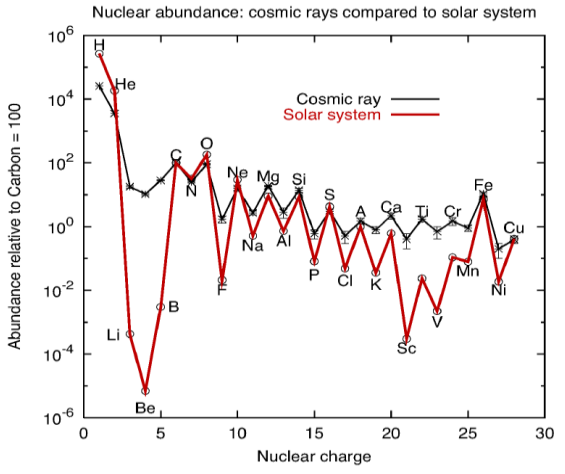

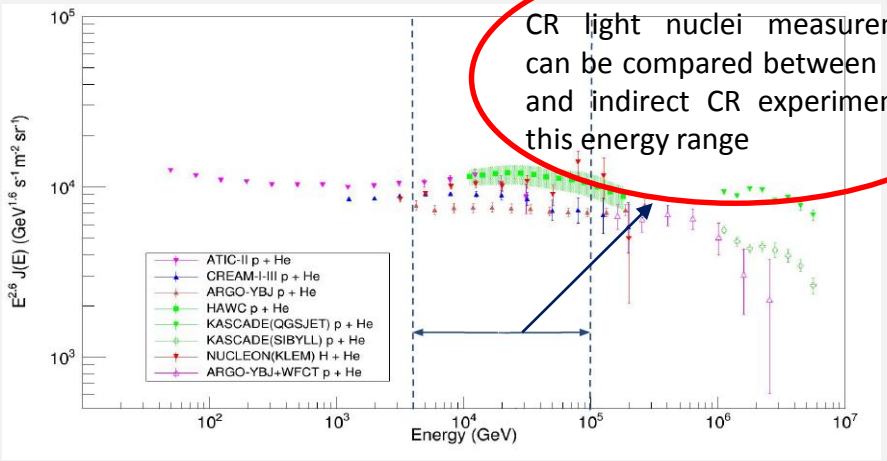

CR light nuclei measurements can be compared between direct and indirect CR experiments at this energy range

PART 02

The DAMPE experiment

Part 2

- DAMPE Collaboration and the detector system
- The Plastic Scintillator Detector (PSD)
- The Silicon Tungsten Tracker (STK)
- The BGO Calorimeter (BGO)
- The Neutron Detector (NUD)

The DAMPE experiment

The DArk Matter Particle Explorer (DAMPE) Collaboration



Launched on December 17th 2015, DAMPE has been collecting CR data for more than 4 years!

- Study the CR electron spectrum
- Study the CR nuclei spectra
- High energy gamma-ray astronomy
- Search for dark matter signatures in lepton spectra

The DAMPE experiment

Scientific results:

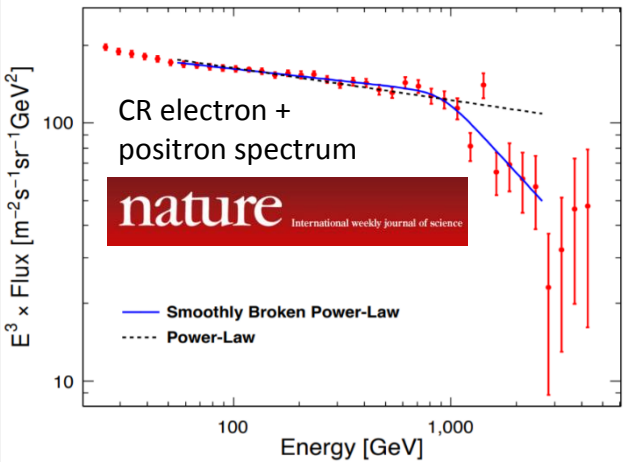

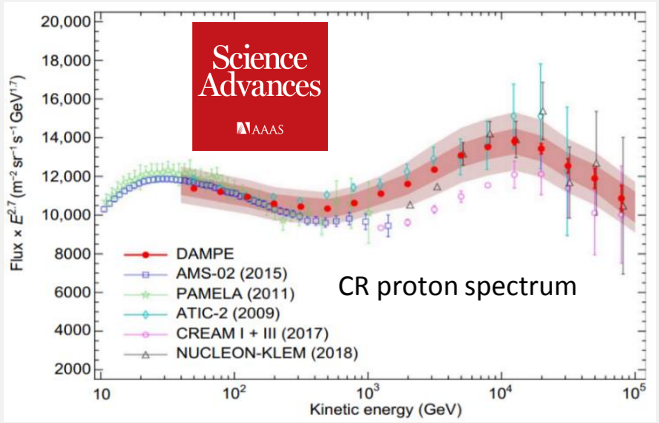

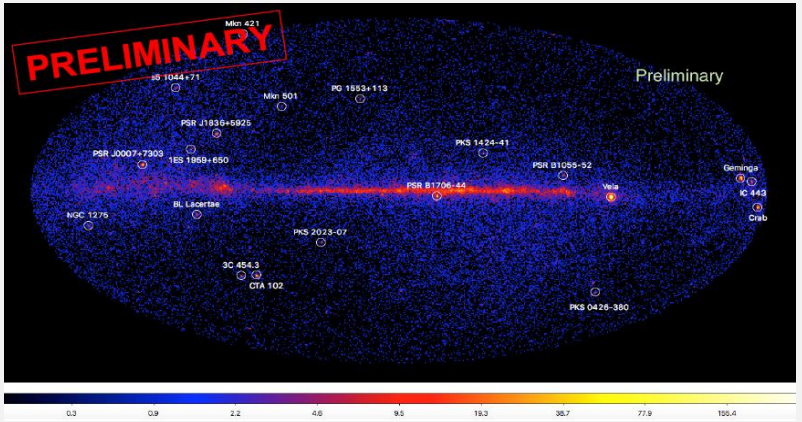

510 days counts map. Mollweide projecti, 0.5°×0.5°pixels
E> 2GeV 90000 events O(20) sources detected

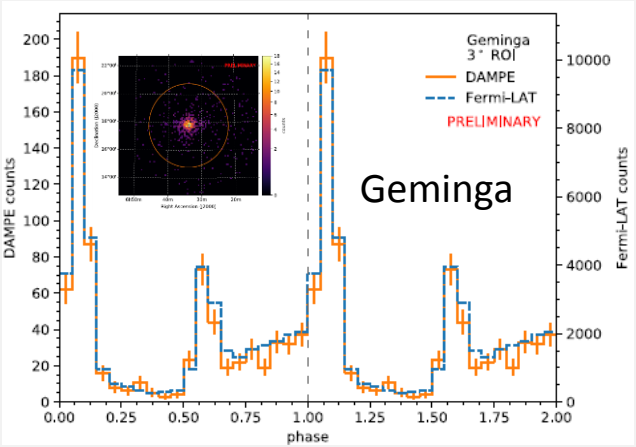

The DAMPE detector system

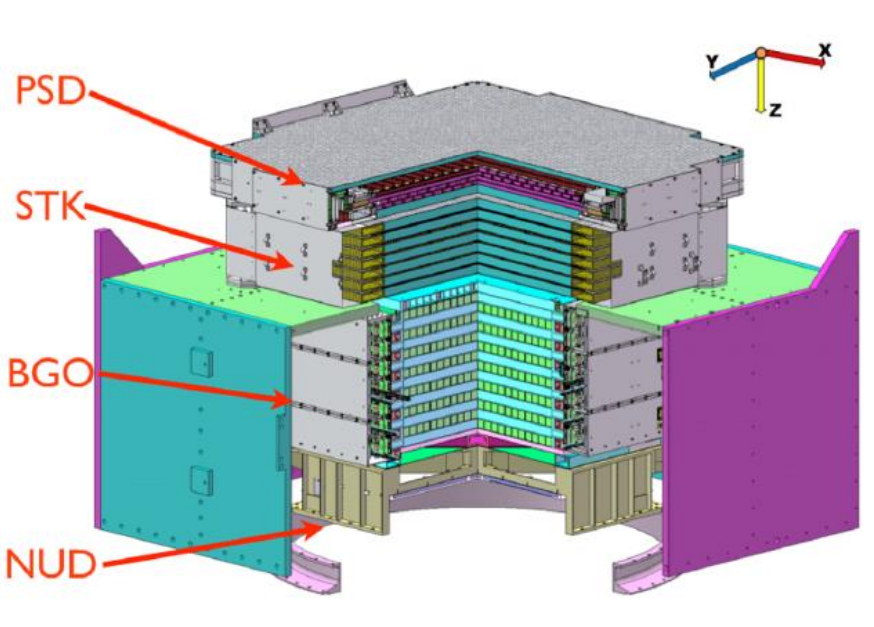

Parameters	Values
Energy range for gamma-rays and electrons	5GeV - 10 TeV
Energy resolution for gamma-rays and electrons	$\leq$ 1.5% at 800 GeV
Energy range for nuclei	50 GeV/n - 100 TeV/n
Energy resolution for nuclei	$\leq$ 40% at 800 GeV
Geometric factor for electrons	$0.3 m^2 \cdot$ sr above 30 GeV
Geometric factor for protons	$0.04 m^2 \cdot$ sr above 100 GeV
Angular resolution for photons	$\leq$ 0.2° at 100 GeV
Field of View	$\sim$ 1.0 sr

Radiation lengths(X_0): 32
Nuclear reaction lengths(λ): 1.6

DAMPE is composed of four sub-detectors:

- The Plastic Scintillator Detector (PSD)
- The Silicon-Tungsten tracKer (STK)
- The Bismuth Germanium Oxide imaging calorimeter (BGO)
- The NeUtron Detector (NUD)

The DAMPE experiment

Part 2

- DAMPE Collaboration and the detector system
- The Plastic Scintillator Detector (PSD)
- The Silicon Tungsten Tracker (STK)
- The BGO Calorimeter (BGO)
- The Neutron Detector (NUD)

PSD

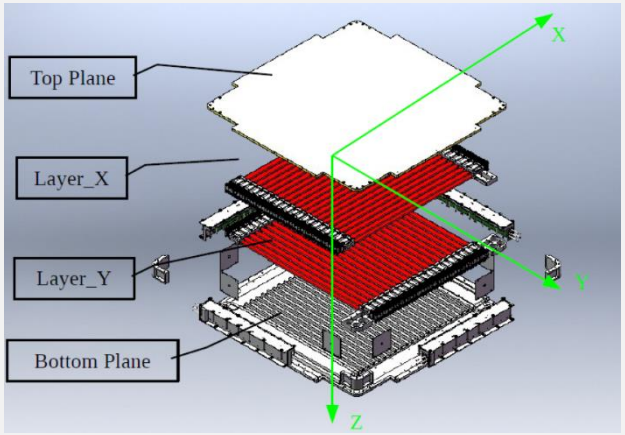

The PSD measures the absolute value of the electric charge (Z) of entering particles, by using the energy release information in the PSD which is proportional to Z^2.

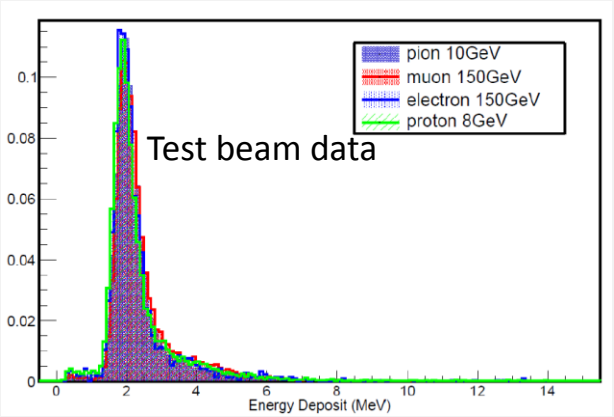

The PSD works as an anticoincidence detector for gamma-rays as well.

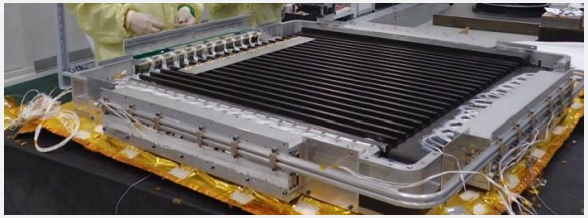

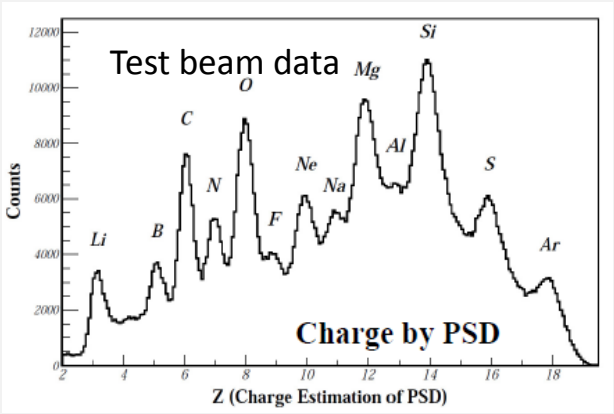

The DAMPE experiment

Part 2

- DAMPE Collaboration and the detector system
- The Plastic Scintillator Detector (PSD)
- The Silicon Tungsten Tracker (STK)
- The BGO Calorimeter (BGO)
- The Neutron Detector (NUD)

The DAMPE experiment

STK

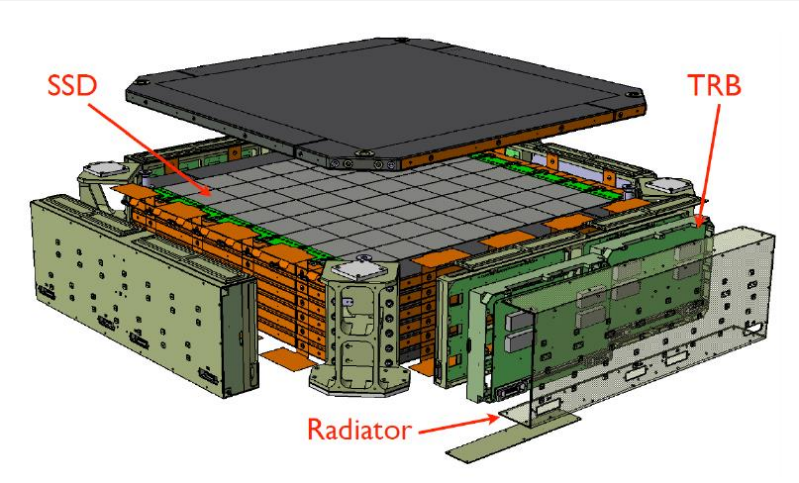

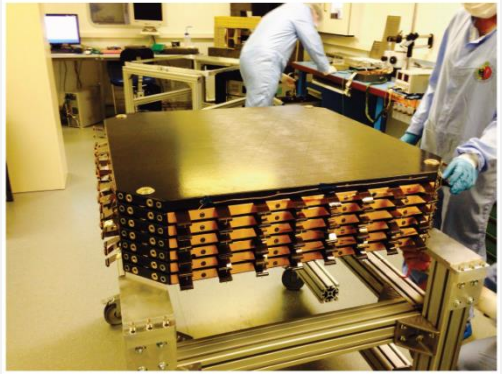

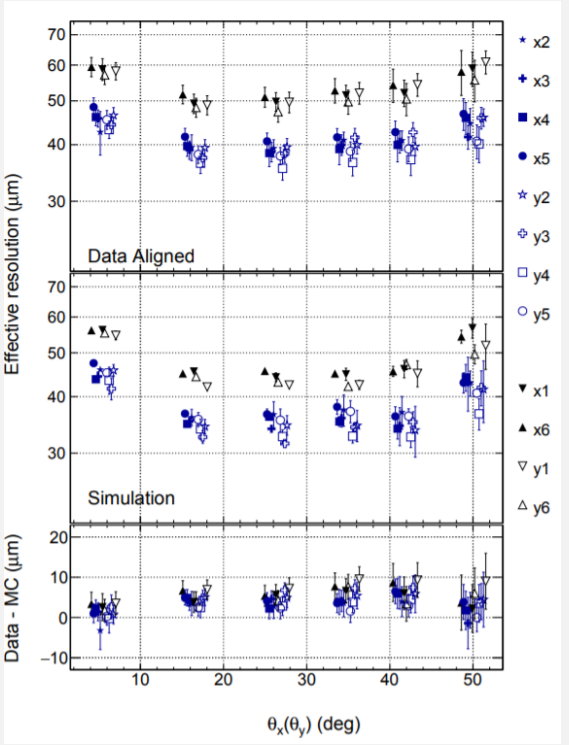

The STK is in charge of reconstructing the tracks of entering particles and converting gamma-rays into electron/positron pairs. Moreover, the STK provides an additional charge measurement for CR nuclei with Z < 9.

The spatial resolution is better than 60 μm for each layer.

The DAMPE experiment

Part 2

- DAMPE Collaboration and the detector system
- The Plastic Scintillator Detector (PSD)
- The Silicon Tungsten Tracker (STK)
- The BGO Calorimeter (BGO)
- The Neutron Detector (NUD)

BGO

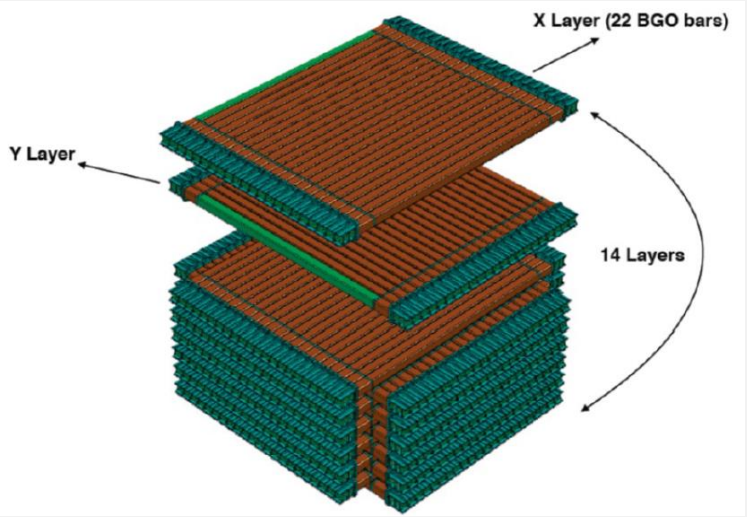

The BGO can also reconstruct the track of an event according to the energy deposition.

The BGO is mainly used to:

- measure the energy of an incident particle
- distinguish lepton and hadron events by using their 3D profile images of the shower
- provide trigger for the data acquisition system

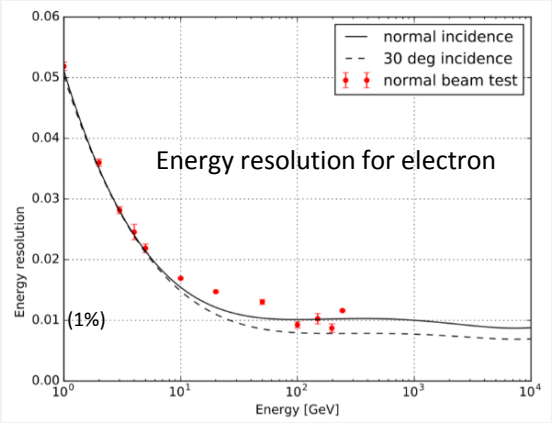

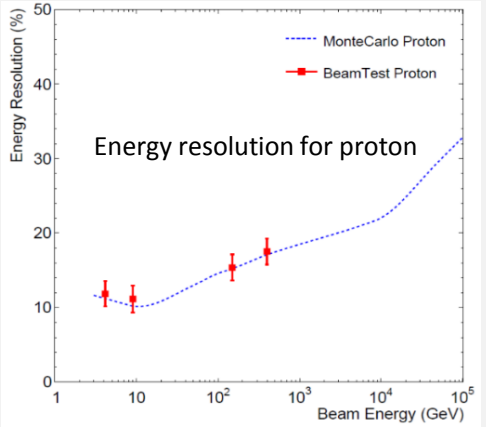

The DAMPE experiment

Part 2

- DAMPE Collaboration and the detector system
- The Plastic Scintillator Detector (PSD)
- The Silicon Tungsten Tracker (STK)
- The BGO Calorimeter (BGO)
- The Neutron Detector (NUD)

NUD

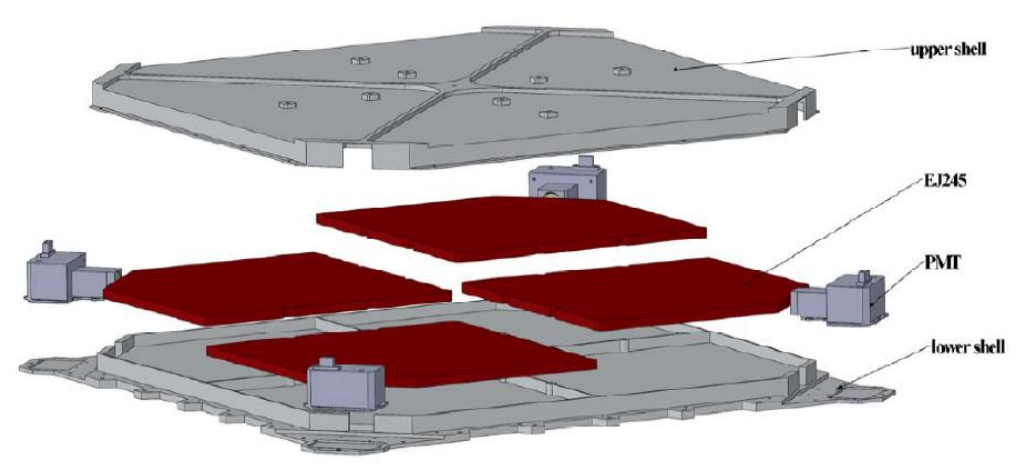

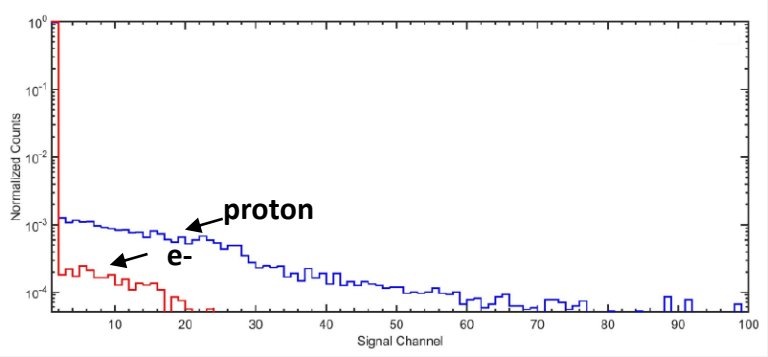

The NUD is used to detect the neutrons produced by hadronic showers. It is composed by four blocks of plastic scintillators doped with ^{10}B nuclei.

$$^{10}\mathrm{B} + \mathrm{n} \rightarrow {}^{7}\mathrm{Li} + \alpha + \gamma$$

The NUD is able to enhance the hadronic shower rejections capability in the search for electrons/positrons or gamma-rays.

PART 03

Energy reconstruction of hadronic showers





Part 3

- Difficulties in hadron energy reconstruction
- Unfolding algorithms
- Test the unfolding algorithms with MC samples
- Test the unfolding algorithm with beam data

Difficulties in hadron energy reconstruction

The difficulties include:

- About 20% of the entering particles will only lose their energy through ionization process
- The shower process has larger intrinsic fluctuations
- Shower containment at the highest energies
- Insufficient experimental data at high energy to testify different hadronic models

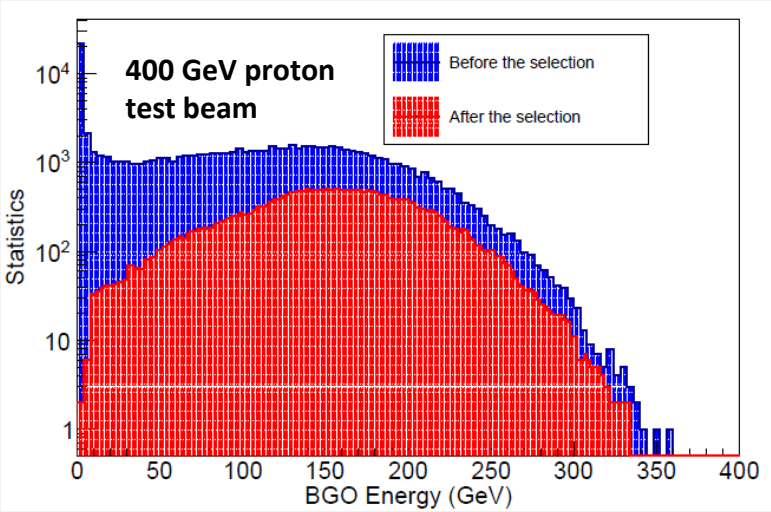

The particles that induce a shower and are well contained by the BGO are selected to decrease the uncertainties.

Part 3

- Difficulties in hadron energy reconstruction with DAMPE
- **Unfolding algorithms**
- Test the unfolding algorithms with MC samples
- Test the unfolding algorithm with beam data

Unfolding algorithms

The energy distribution of events we observe through the BGO ($\Phi(E_{\mathrm{BGO}})$) is the primary energy distribution of these events ($\Phi(E_{\mathrm{T}})$) convolute the detector response($R(E_{\mathrm{BGO}}, E_{\mathrm{T}})$) effect as:

$$\Phi(E_{\mathrm{BGO}}) = \int R(E_{\mathrm{BGO}}, E_{\mathrm{T}}) \cdot \Phi(E_{\mathrm{T}}) \cdot dE_{\mathrm{T}}$$

The discontinuous form of the equation is:

$$N\left(E_{\mathrm{BGO}}^{j}\right) = \sum_{n}^{i} P(E_{\mathrm{BGO}}^{j} | E_{\mathrm{T}}^{i}) \cdot N\left(E_{\mathrm{T}}^{i}\right) \qquad j = 1,2,3 \ldots m$$

The $N\left(E_{\mathrm{BGO}}^{j}\right)$ can be obtained from the detector, then $N\left(E_{\mathrm{T}}^{i}\right)$ is our goal. This becomes an unfolding problem.

Unfolding algorithms

$P(E^j_{\mathrm{BGO}}|E^i_{\mathrm{T}})$(Response matrix) $\longrightarrow$ $P(E^i_{\mathrm{T}}|E^j_{\mathrm{BGO}})$ (Unfolding matrix)

So:

$$N\left(E^i_{\mathrm{T}}\right) = \sum_n^i P(E^i_{\mathrm{T}}|E^j_{\mathrm{BGO}}) \cdot N\left(E^j_{\mathrm{BGO}}\right) \quad j = 1,2,3 \ldots m$$

Bayesian method:

$$P\left(E^i_{\mathrm{T}}\middle|E^j_{\mathrm{BGO}}\right) = \frac{P(E^j_{\mathrm{BGO}}|E^i_{\mathrm{T}})\cdot P_0(E^i_{\mathrm{T}})}{\sum_{i=1}^n P(E^j_{\mathrm{BGO}}|E^i_{\mathrm{T}})\cdot P_0(E^i_{\mathrm{T}})}$$

Once the primary energy distribution ($N\left(E^i_{\mathrm{T}}\right)$) is obtained, the flux can be derived as:

$$\Phi(E, E+\Delta E) = \frac{N(E^i_{\mathrm{T}})}{\Delta T \cdot A_{acc} \cdot \Delta E}$$

Bayes unfolding algorithms

1. Compute $P(E^j_{\mathrm{BGO}}|E^i_{\mathrm{T}})$ from the MC samples
2. Compute $P_0(E^i_{\mathrm{T}})$ from the previous experiments
3. Compute $P\left(E^i_{\mathrm{T}}\middle|E^j_{\mathrm{BGO}}\right)$ through Bayes equation
4. Derive the spectrum, if the spectrum agrees with the expectation, stop the iteration. Else go to step 5
5. Use the derived flux to compute the $P_0(E^i_{\mathrm{T}})$, then go to step 3 with the new $P_0(E^i_{\mathrm{T}})$ and starts a new iteration

The Bayes unfolding algorithm will be first tested with MC samples, together with the Singular Value Decomposition (SVD) method and Iterative Dynamically Stabilized (IDS) method.

Part 3

- Difficulties in hadron energy reconstruction
- Unfolding algorithms
- Test the unfolding algorithms with MC samples
- Test the unfolding algorithm with beam data

Test the unfolding algorithms with MC samples

The fit function of the proton flux measured by AMS-02 will be used to produce the simulated spectrum.

The simulation is based on 12.8×10^8 MC samples: Half for the response matrix, half for the spectrum.

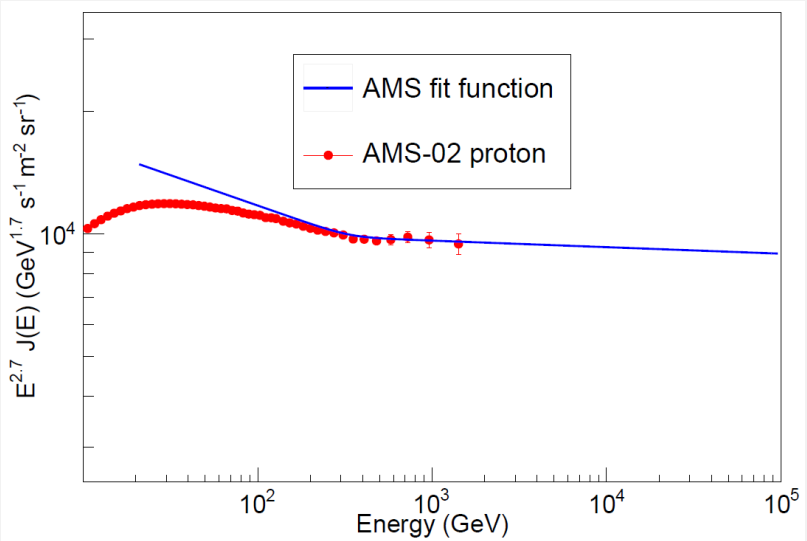

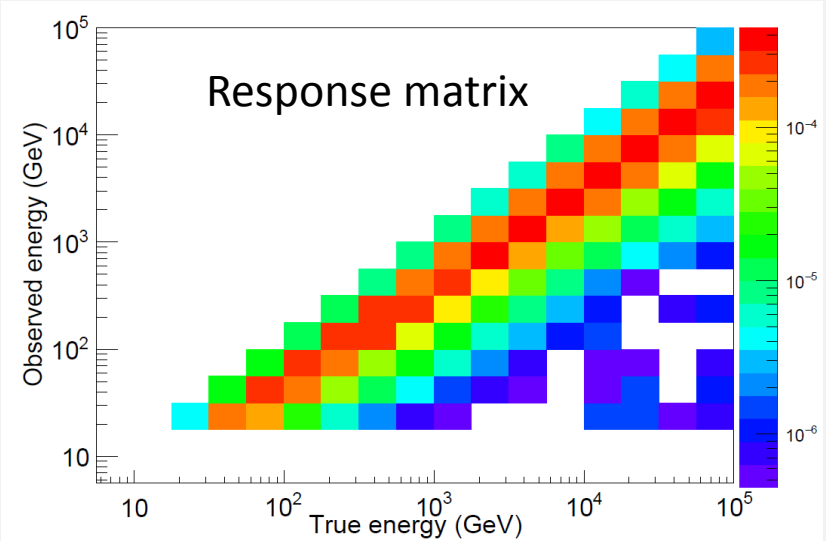

Test the unfolding algorithms with MC samples

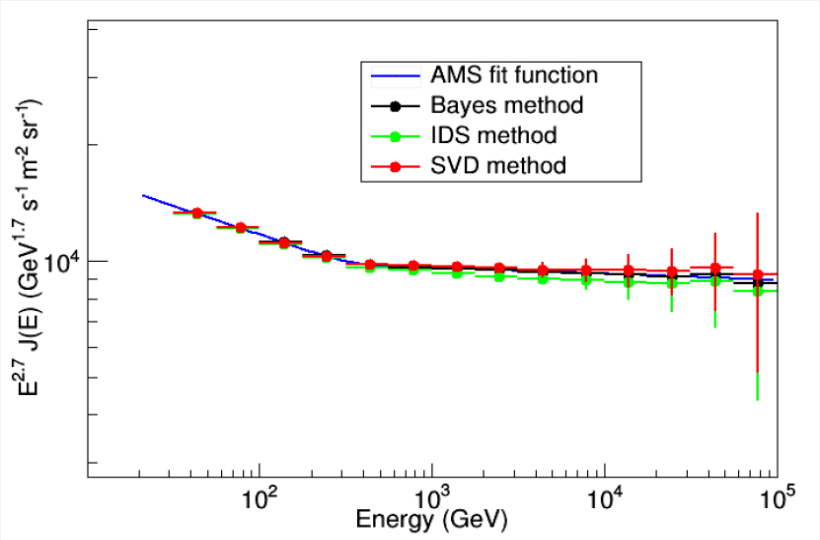

All the three methods can reconstruct the spectra quite close to the expectation.

The Bayes method has the best performance.

The ratios between the reconstructed results and the fit function show that the Bayes method has a bias less than 2%, meanwhile, the other two methods have a bias within 5% .

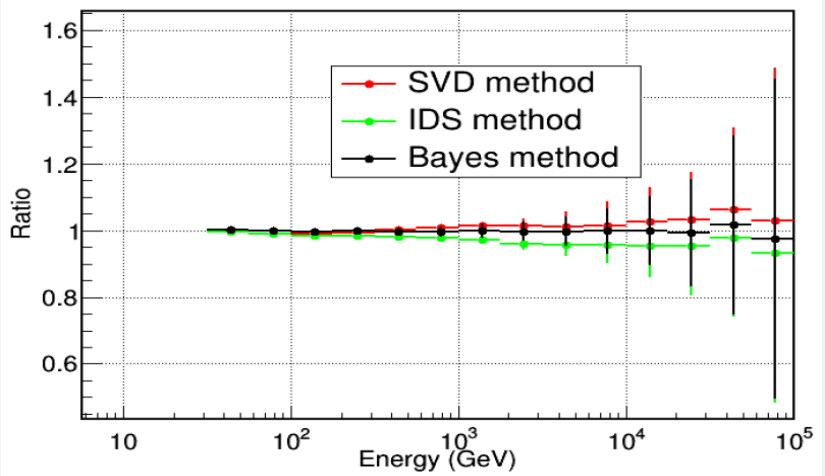

Part 3

- Difficulties in hadron energy reconstruction
- Unfolding algorithms
- Test the unfolding algorithms with MC samples
- Test the unfolding algorithm with beam data

Test the unfolding algorithm with beam data

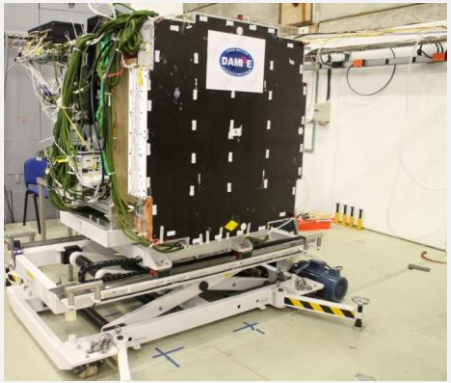

Both the MC and data (at CERN SPS) of the **400 GeV proton beam** test are used to test the Bayes unfolding method.

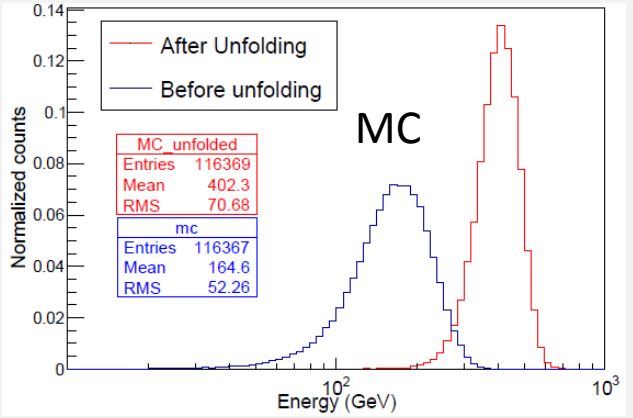

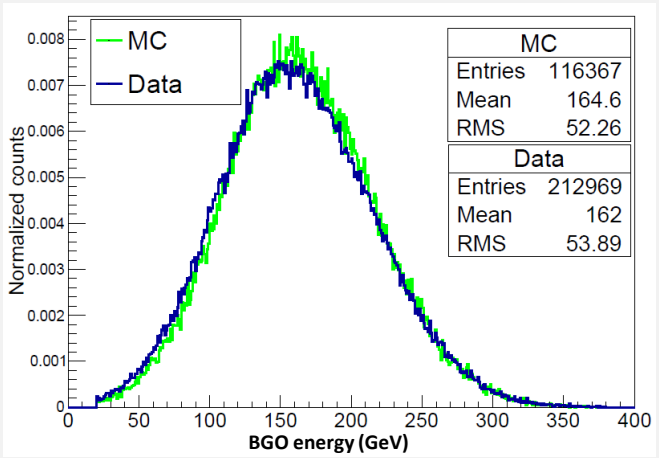

The mean value of the distributions for both the MC and data after the unfolding are around 400 GeV.

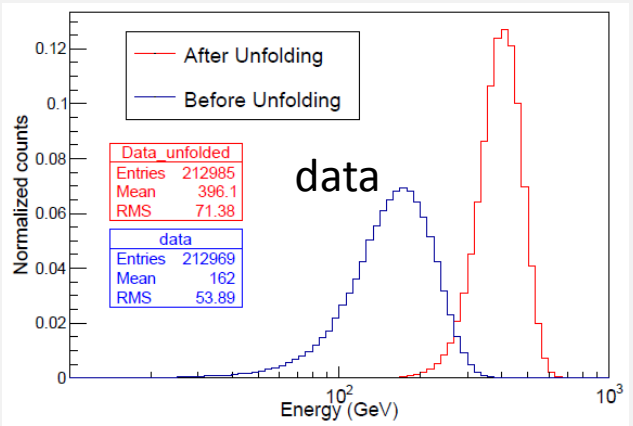

Test the unfolding algorithms with beam data

The unfolding result of the **150 GeV Proton beam** data.

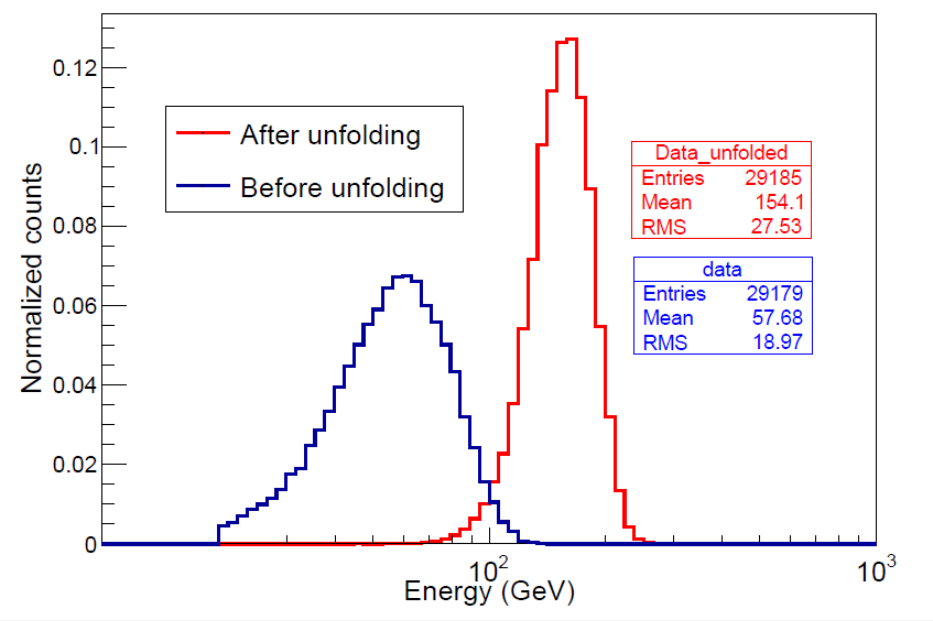

The energy resolutions are 17.86% for 150 GeV proton and 18.02% for 400 GeV proton, which agrees with the simulation.

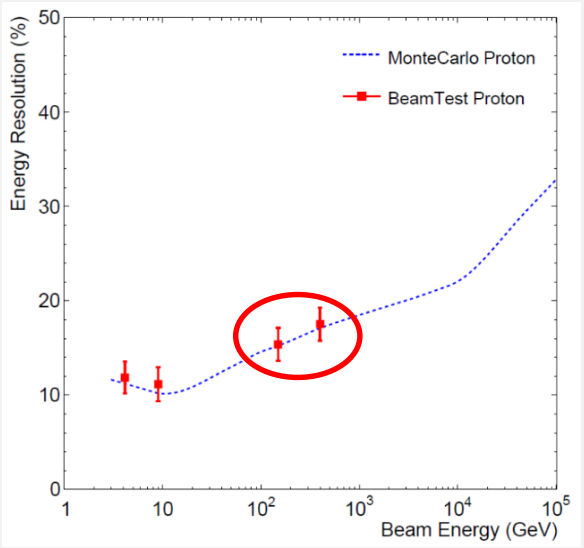

PART 04

Measurement of the H + He flux

Measurement of the H + He flux

Part 4

- Overview on the flux calculation
- Calculation of the exposure time
- Calculation of the effective acceptance
- Uncertainties and the final spectrum

Overview on the flux calculation

The flux in an energy interval can be derived as:

$$\Phi(E, E+\Delta E)=\frac{N_{\mathrm{H+He}}(E,E+\Delta E)}{\Delta T \cdot A_{acc} \cdot \Delta E}$$

$N_{\mathrm{H+He}}(E, E+\Delta E)$: After event selection and energy reconstruction, the number of the candidates in energy interval of $[E, E+\Delta E]$;

ΔT: Exposure time;

A_{acc}: Detector effective acceptance in energy interval of $[E, E+\Delta E]$;

ΔE: Energy span for a certain energy bin.

Measurement of the H + He flux

Part 4

- Overview on the flux calculation
- Calculation of the exposure time
- Calculation of the effective acceptance
- Uncertainties and the final spectrum

Measurement of the H + He flux

Calculation of the exposure time

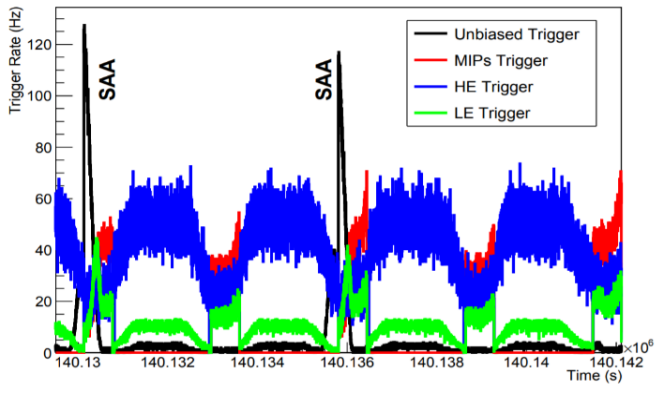

The trigger rates in two consecutive orbit flights

On average, trigger rate is ~50 Hz, and DAMPE can collect ~5 million CR events every day.

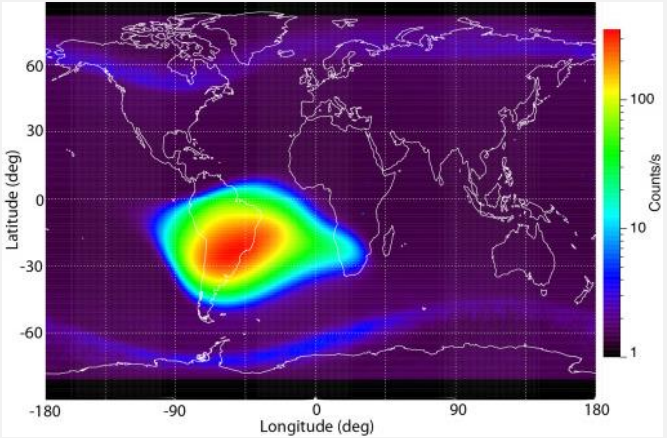

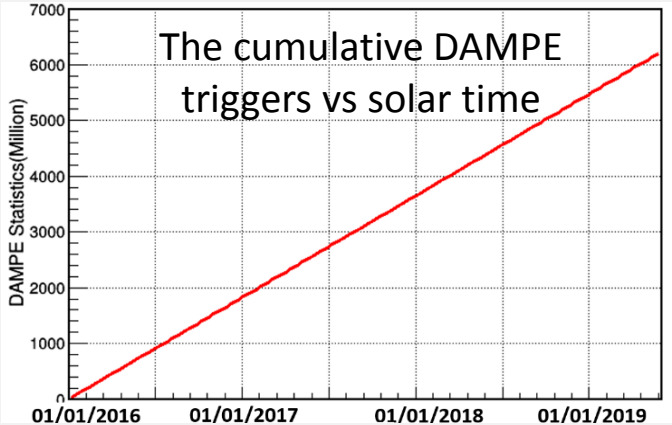

The data obtained in the South Atlantic Anomaly (SAA) will not be used in the analysis.

Calculation of the exposure time

The data collected between 01/01/2016 and 31/03/2019 (39 months) are used.

The contribution to the “dead time” comes from:

- When DAMPE was passing through the SAA region (4.5%)
- The detector response time (18%)
- The detector calibration (1.8%)
- The days of 8-13/09/2017, due to an intense solar flare and the days of 29-30/12/2017, due to a high voltage reset in DAMPE, have been removed from the total days

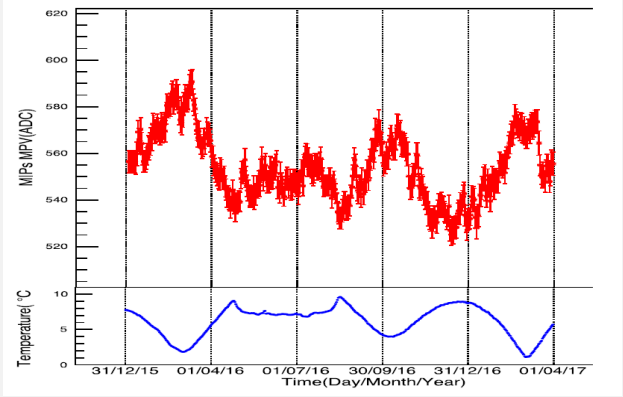

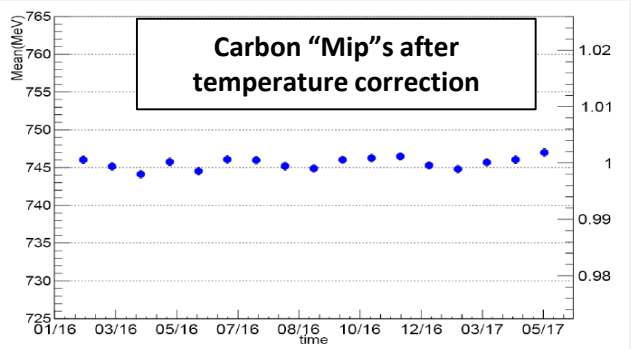

The exposure time accounts for 75.54% of the total orbit time and equals 5.9×10^7 s, which is equivalent to 683 days.

Measurement of the H + He flux

Part 4

- Overview on the flux calculation
- Calculation of the exposure time
- Calculation of the effective acceptance
- Uncertainties and the final spectrum

Calculation of the effective acceptance

The effective acceptance in i-th energy bin (A_{acc}^{i}) is derived as:

$$A_{acc}^{i} = G_{gen} \cdot \frac{N(E_T^i, sel)}{N(E_T^i)}$$

- G_{gen} : Geometric acceptance
- $N(E_T^i)$: The number of generated event in i-th bin of primary energy in MC samples
- $N(E_T^i, sel)$: The number of surviving event in i-th bin of primary energy after the selection cuts in MC samples

In order to calculate the effective acceptance, the selection procedures based on the MC simulation is the key point.

Calculation of the effective acceptance—MC simulation.

The detector response was simulated by using the GEANT4 package, also made cross checks with FLUKA. At low energy, two physics lists (representing two different hadronic interaction models) were tested: FTFP_BERT (FTFP) and FTFP_QGSP_BERT (QGSP).

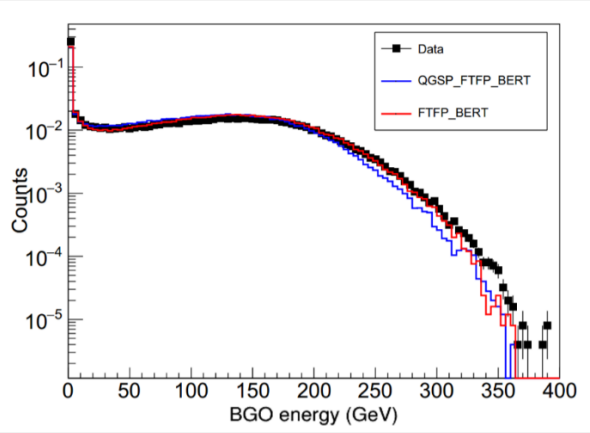

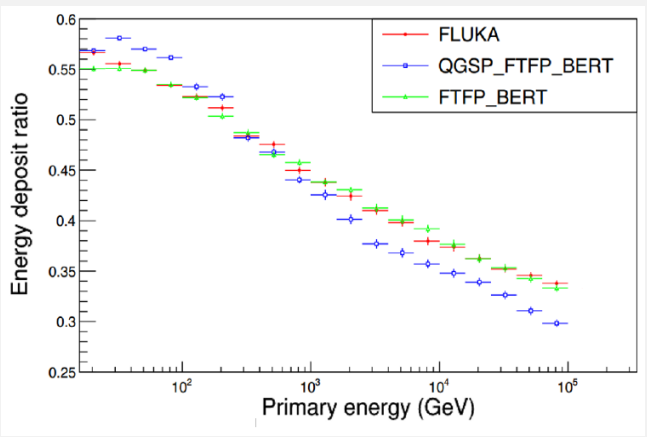

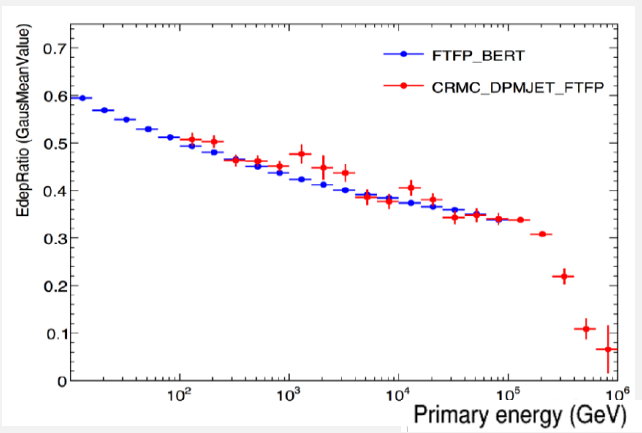

Based on data-MC comparisons, the FTFP model was chosen as reference. The FTFP model also has a better agreement with FUKA. At higher energies (> 100 TeV for H) the CRMC package with DPMJET + FTFP model was used.

Calculation of the effective acceptance—data selection

There are five selection steps

- Pre-selection
- Track selection
- Trigger selection and shower development.
- Removal of electron/positron particles
- Charge selection

The same selections are used on both MC and orbit data

Calculation of the effective acceptance—data selection

Pre-selection: Based on the BGO measurement, it guarantees a shower being well contained by the calorimeter and removes the events influenced by the geomagnetic cutoff.

Track selection: Normally, there will be more than one track being reconstructed for an event. The best track is selected for each event.

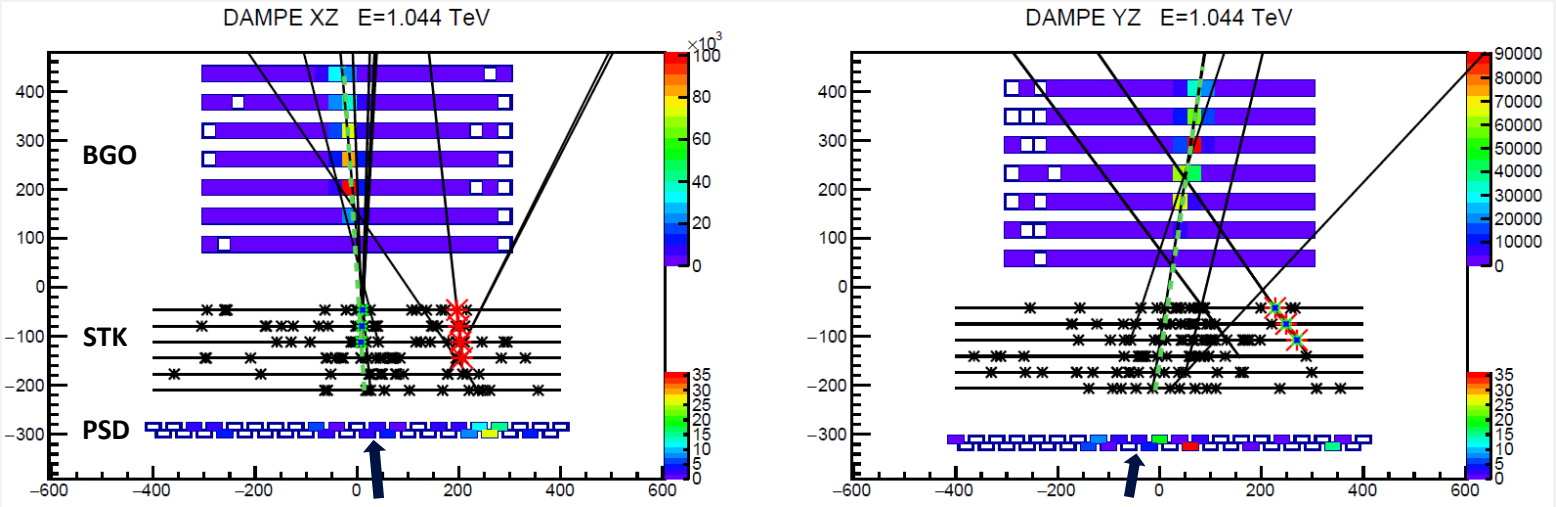

Calculation of the effective acceptance—data selection

Trigger selection and shower development: The event must activate the High Energy Trigger (HET) of DAMPE. Besides, its energy deposition in the first and second layer of the BGO must be less than that in third and fourth layer.

Removal of electron and positron particles: Based on the shower shape, the leptons and hadrons can be well separated.

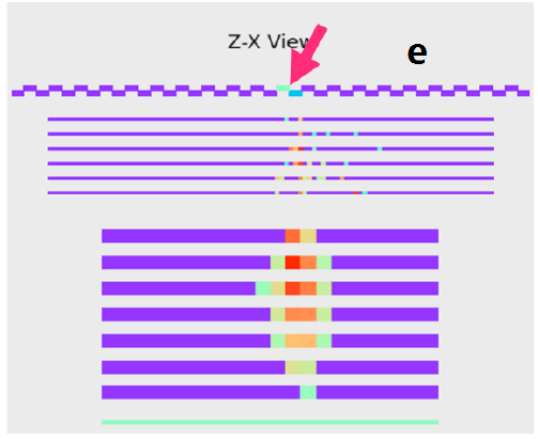

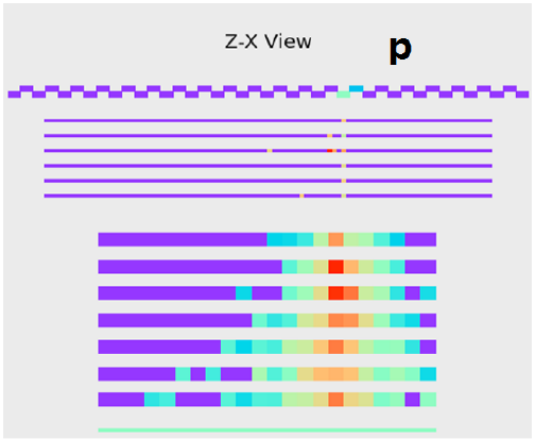

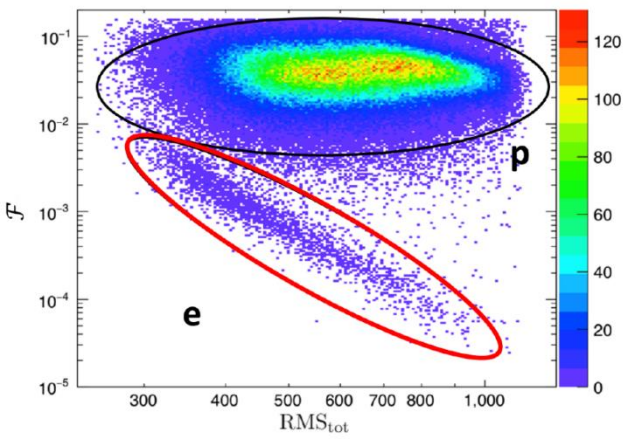

Calculation of the effective acceptance—data selection

Charge selection

The PSD measurements are used

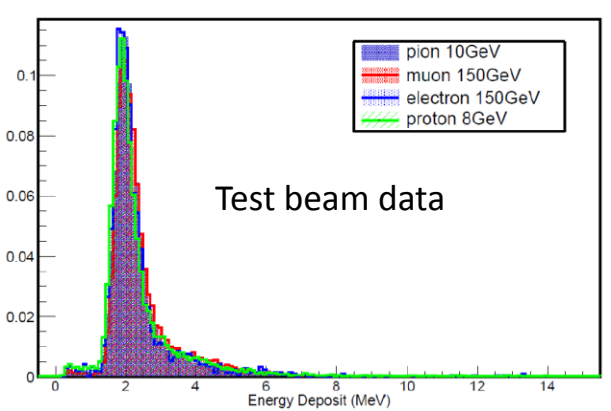

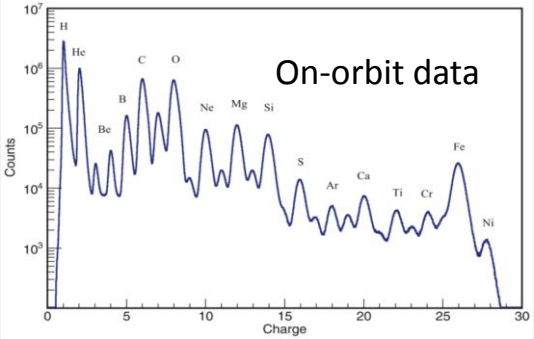

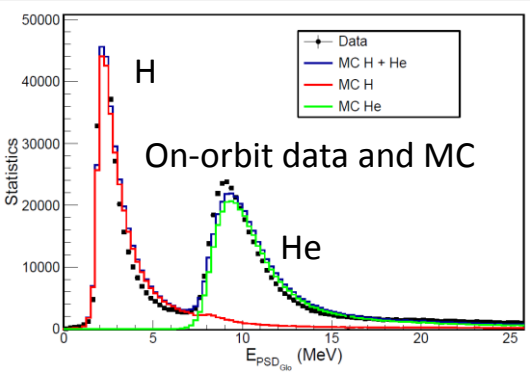

Due to the very high energy of the detected CR cosmic protons and helium, the relativistic rise of the energy release in the PSD has to be taken into account.

Calculation of the effective acceptance—data selection

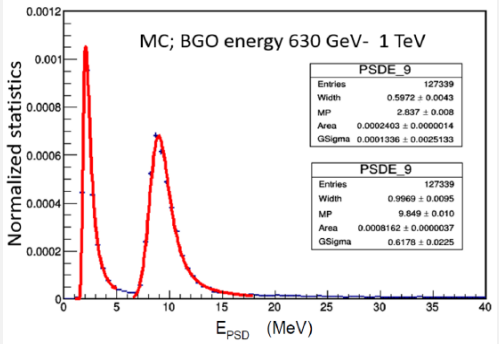

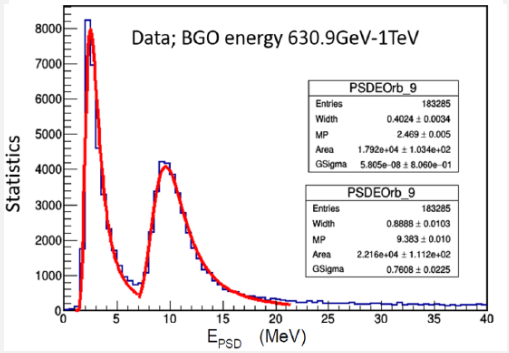

The distributions of E_{PSD} are fitted with a Landau convoluted Gauss function regarding different BGO energy (deposited energy) bins.

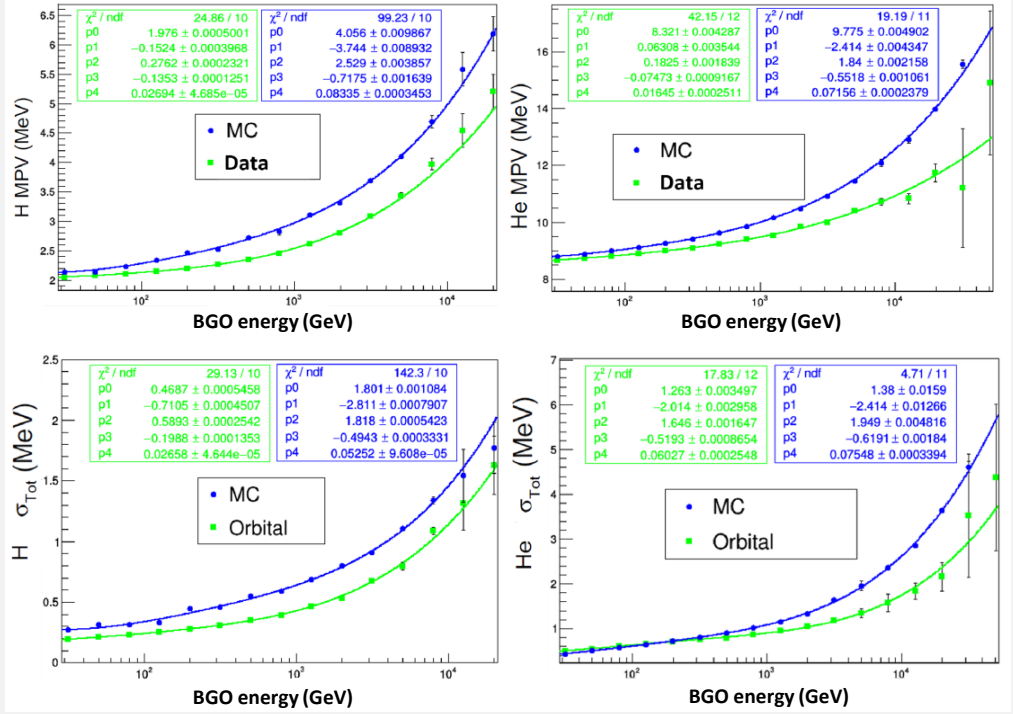

The MPV and sigma of the fitting results with different BGO energy bins show a disagreement between the MC and data.

Measurement of the H + He flux

Calculation of the effective acceptance—data selection

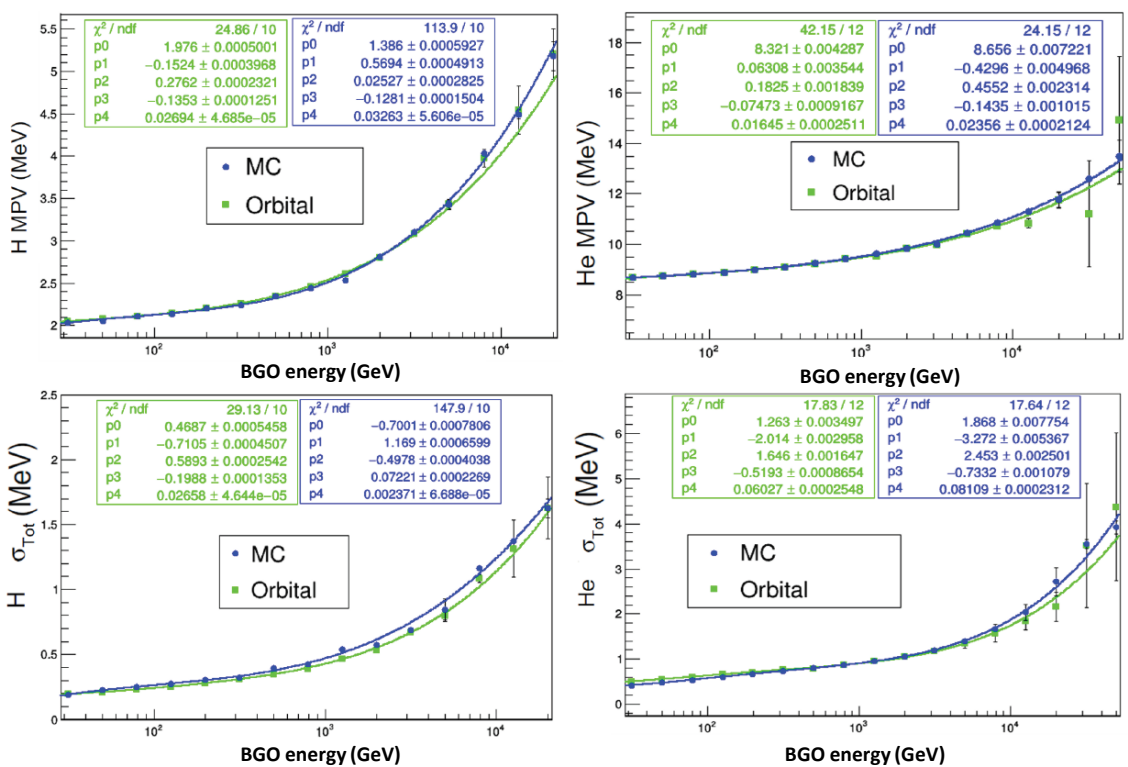

The PSD measurement of MC is corrected event by event to approach the real data.

After correction, the MC and data are in a good agreement.

Calculation of the effective acceptance—data selection

The selection interval for H + He candidates is decided as:

$[f_{\text{H-MPV}}(E_{\text{BGO}})\text{-}3*f_{\text{H-Sigma}}(E_{\text{BGO}}),\ \ f_{\text{He-MPV}}(E_{\text{BGO}})\text{+}6*f_{\text{He-Sigma}}(E_{\text{BGO}})]$

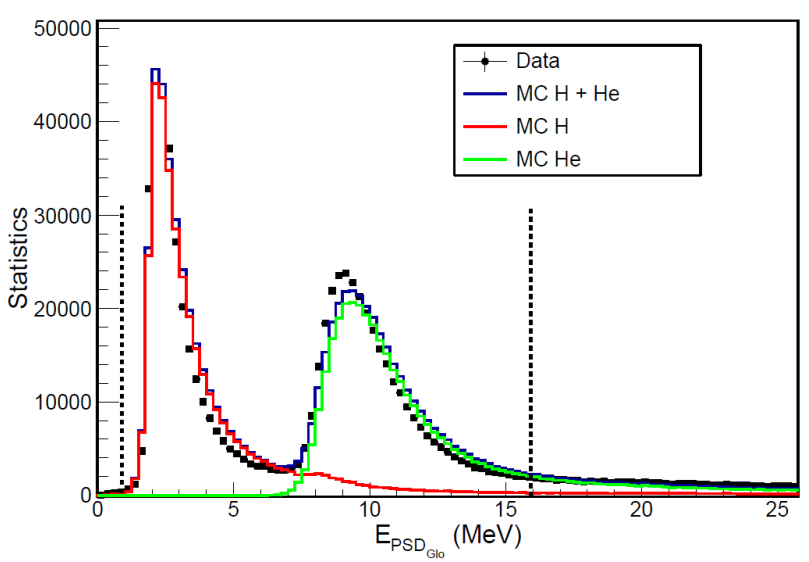

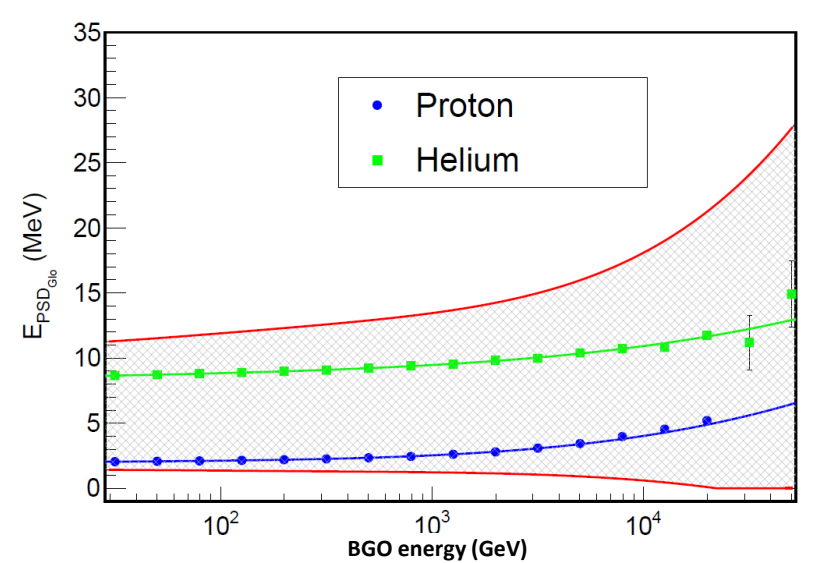

Calculation of the effective acceptance

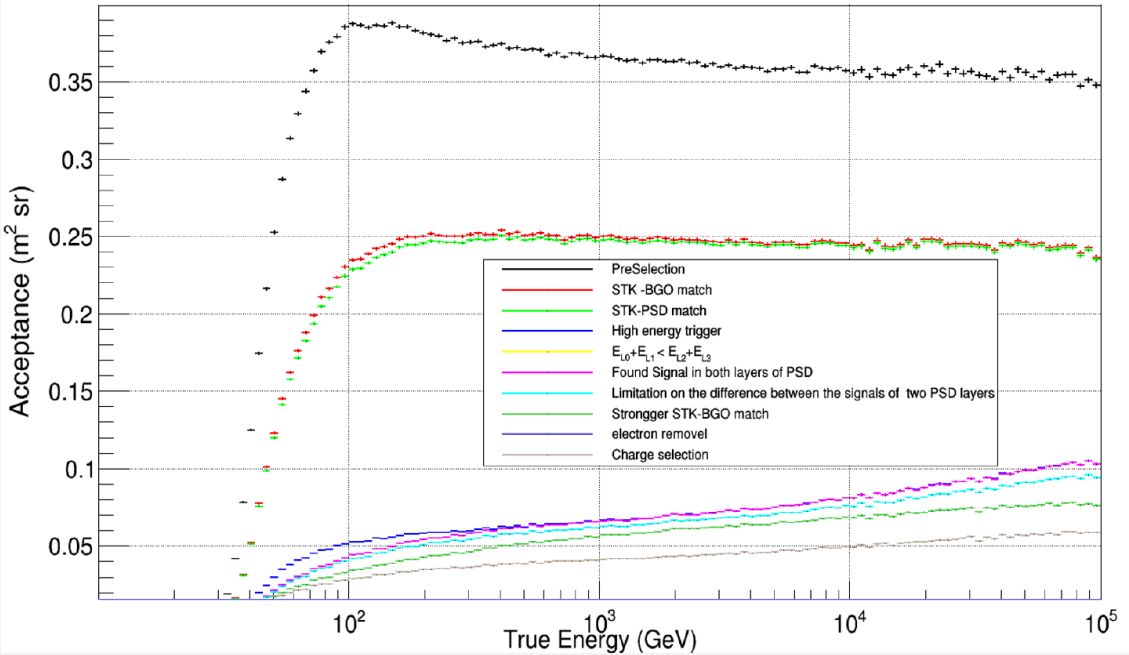

$$A^i_{acc} = G_{gen} \cdot \frac{N(E^i_T, sel)}{N(E^i_T)}$$

The effective acceptance is ~0.05 m^2 sr at 10 TeV after performing all the selections.

Measurement of the H + He flux

Part 4

- Overview on the flux calculation
- Calculation of the exposure time
- Calculation of the effective acceptance
- Uncertainties and the final spectrum

Uncertainties

Due to the large acceptance, DAMPE measurements have statistical uncertainties very small compared to previous direct experiments in the same energy range. Meanwhile, the systematic uncertainties in this analysis could come from:

- The acceptance evaluation
- The ratio between MC H and He in the response matrix
- The hadronic model
- The PSD correction in the MC

Uncertainty--effective acceptance

For the acceptance part, three groups of the selection efficiency will be estimated:

- The High Energy Trigger (HET) efficiency
- The track selection efficiency
- The charge reconstruction efficiency

HET selection efficiency: $\epsilon_{\mathrm{HET}} = \frac{N(\mathrm{HET}|\mathrm{Unb})}{N(\mathrm{Unb})}$

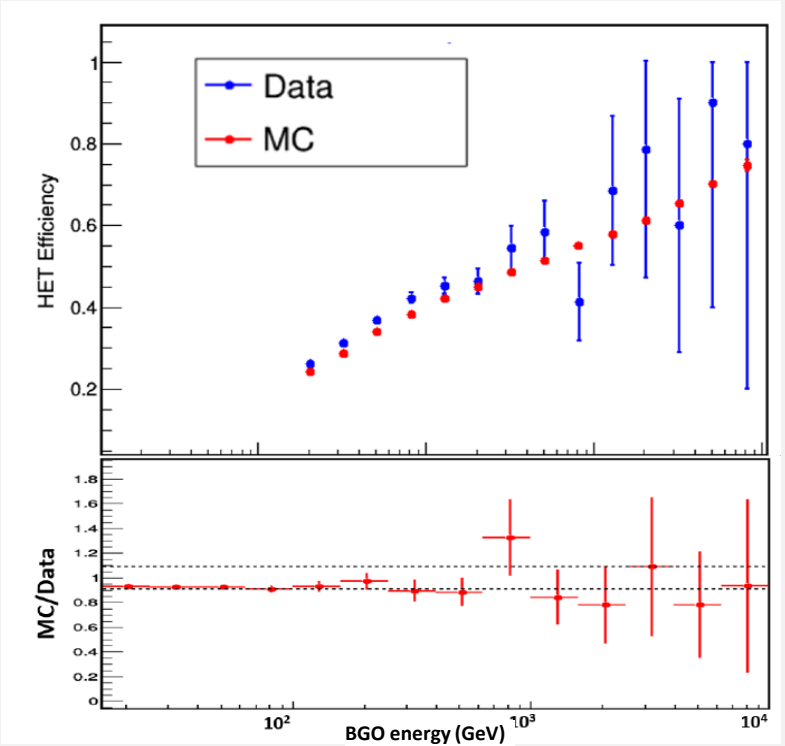

The difference between MC and data is within 6%.

Uncertainty--effective acceptance

The track selection efficiency:

$$\epsilon_{\text{Track}} = \frac{N(\text{STK}|\text{BGO})}{N(\text{BGO})}$$

The difference between MC and data is within 4%.

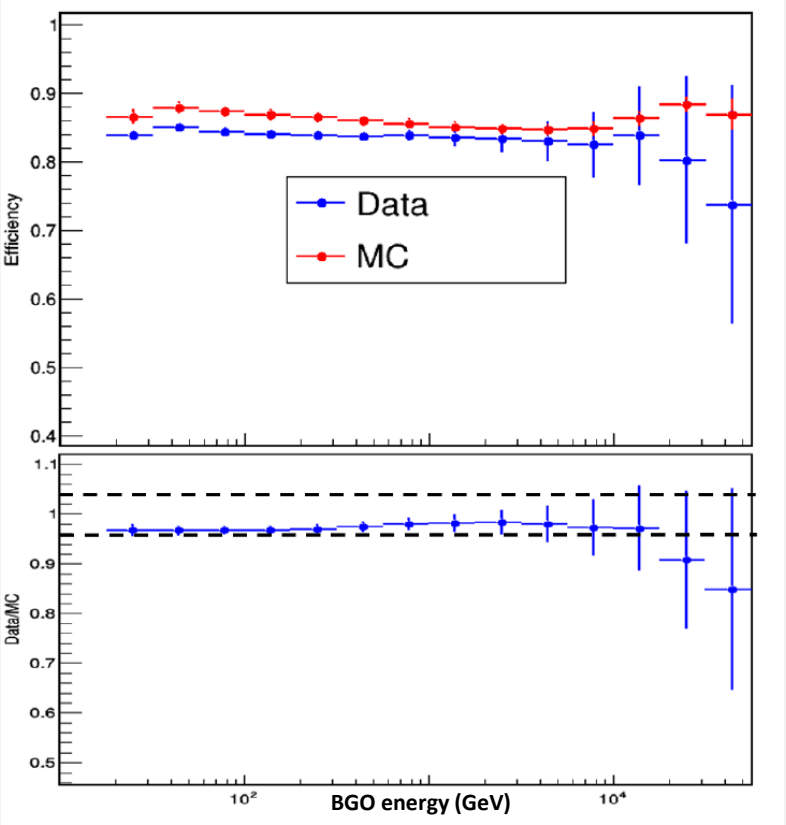

Uncertainty--effective acceptance

The charge reconstruction efficiency:

$$\epsilon_{\mathrm{PSDX}} = \frac{N(\mathrm{PSDX}|\mathrm{PSDY}|\mathrm{STK})}{N(\mathrm{PSDY}|\mathrm{STK})}$$

$$\epsilon_{\mathrm{PSDY}} = \frac{N(\mathrm{PSDY}|\mathrm{PSDX}|\mathrm{STK})}{N(\mathrm{PSDX}|\mathrm{STK})}$$

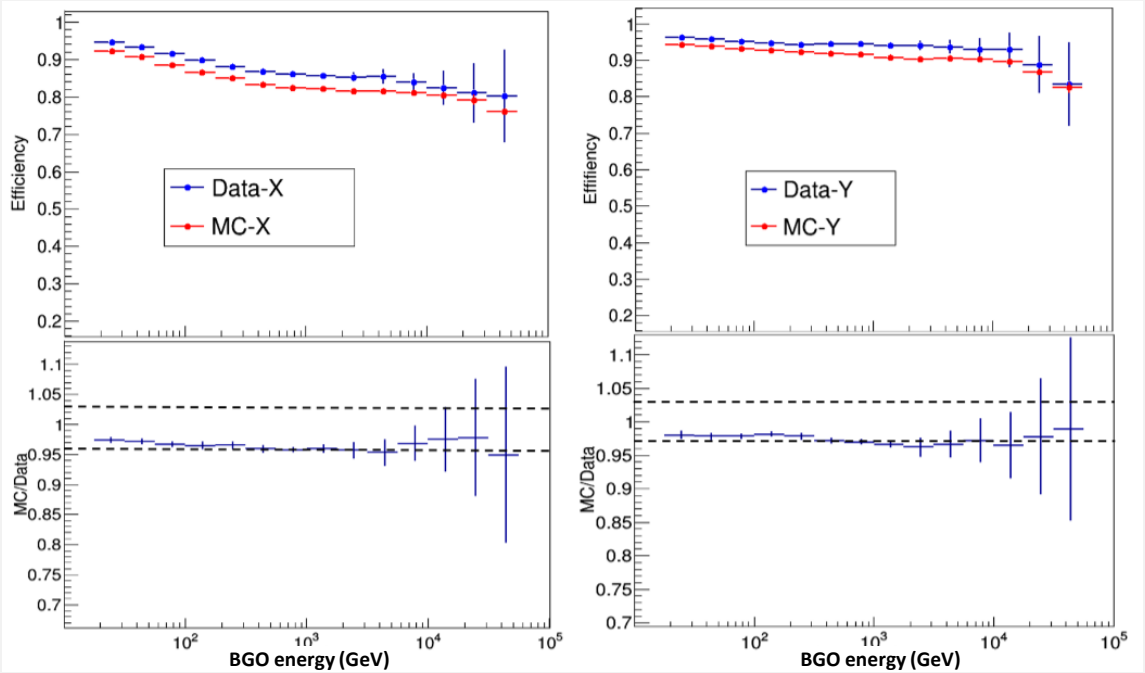

The differences between MC and data for PSD Y layer is within 3%, meanwhile, for PSD X layer is within 4%.

Uncertainty--effective acceptance

In order to transfer the uncertainties to the primary energy, the unfolding should be performed:

$$N(E_T^i)=\sum_{j=1}^{n} P(E_T^i|E_{BGO}^j)\cdot R_{Sel}^j \cdot N\left(E_{BGO}^j\right),\ j=1,2,\dots$$

R_{Sel}^j is the ratio between the MC and data selection efficiency, The overall systematic uncertainties result from these effects are 8.24%.

Uncertainty--H-He ratio

The response matrix $P\left(E_{BGO}^{j}\middle|E_{T}^{i}\right)$ is produced by MC H and He MC samples. The ratio between the H and He could affect the unfolding results.

Three spectra are produced based on different H-He ratio:

- AMS-02 (< 1 TeV) + CREAM-03(> 1 TeV)
- PAMELA(< 1 TeV) + NUCLEON(> 1 TeV)
- ATIC-02

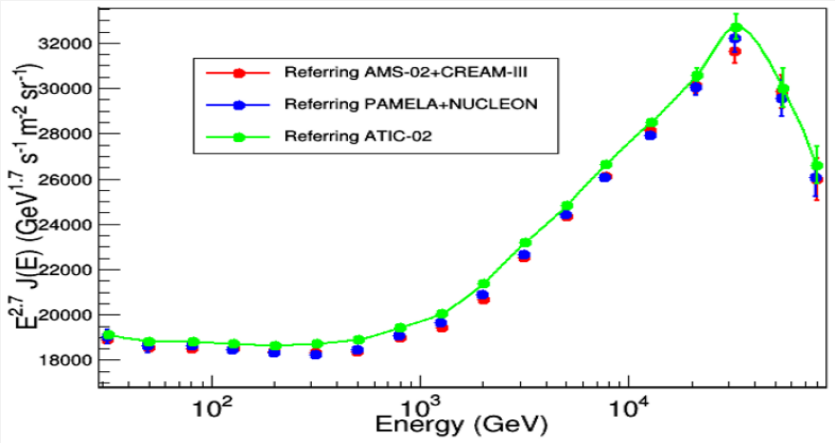

The largest differences come from the ATIC-02 and AMS-02+ CREAM-III based results:

Energy(GeV)	40-300	300-10000	10000-100000
uncertainties	1%	2%	1%

The difference will be taken as the systematic uncertainty.

Uncertainty--hadronic model

The MC simulation with QGSP model is used to derive the spectrum.

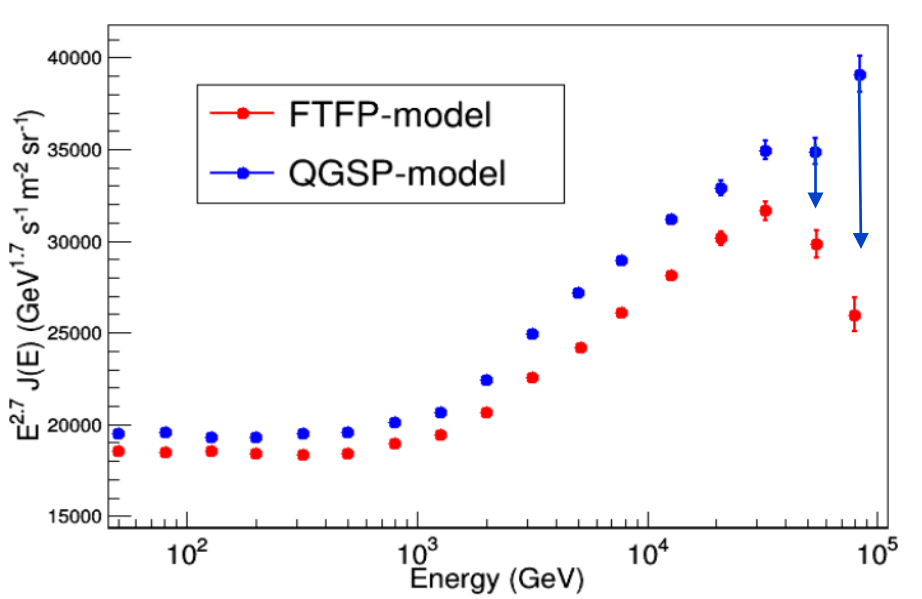

Energy(GeV)	39.8-1584.8	1584.8-2511.8	2511.8-100000.0
uncertainties	5%	7.4%	10%

Despite the last two points, the spectral difference is stable at ~10% after 2 TeV.

The last two data points of the QGSP-model spectrum are the upper limit of the possible values (due to the lack of simulations above 100 TeV).

Uncertainty--the PSD correction

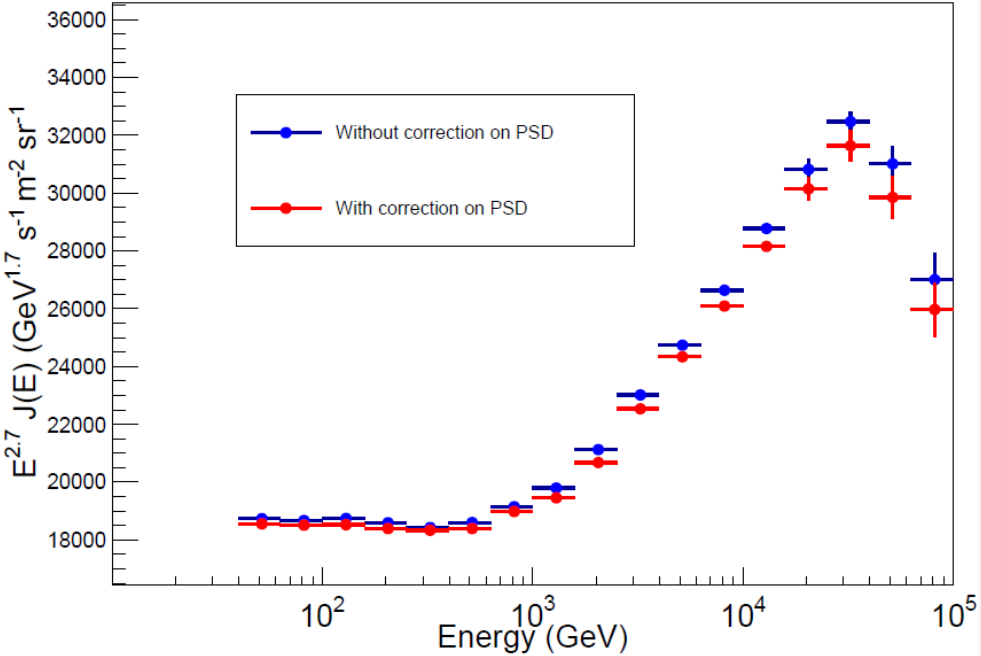

The spectral differences between the results with and without the PSD correction are as follows:

Energy(TeV)	<10.0	10.0-39.81	39.81-100.0
uncertainty	1%	2%	3%

The difference will be taken as the systematic uncertainty.

The PSD correction has a larger influence on proton only and helium only spectrum.

Uncertainties

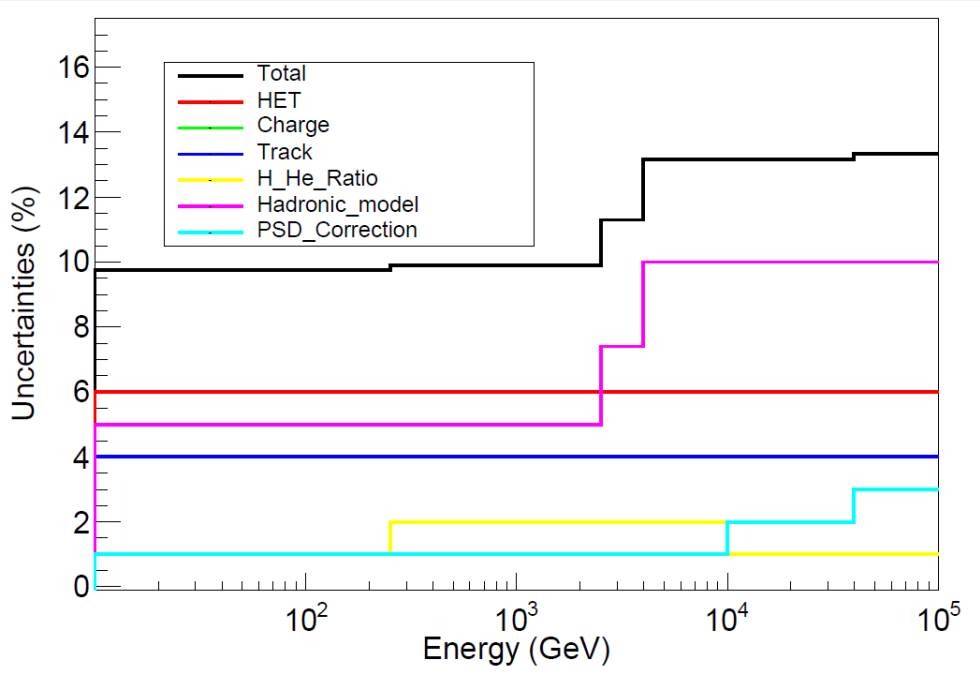

At energy region less than 2.5 TeV, the uncertainty is around 9.5%, then it grows with an increasing energy and gets stable at around 13% after 4 TeV.

Measurement of the H + He flux

Final spectrum

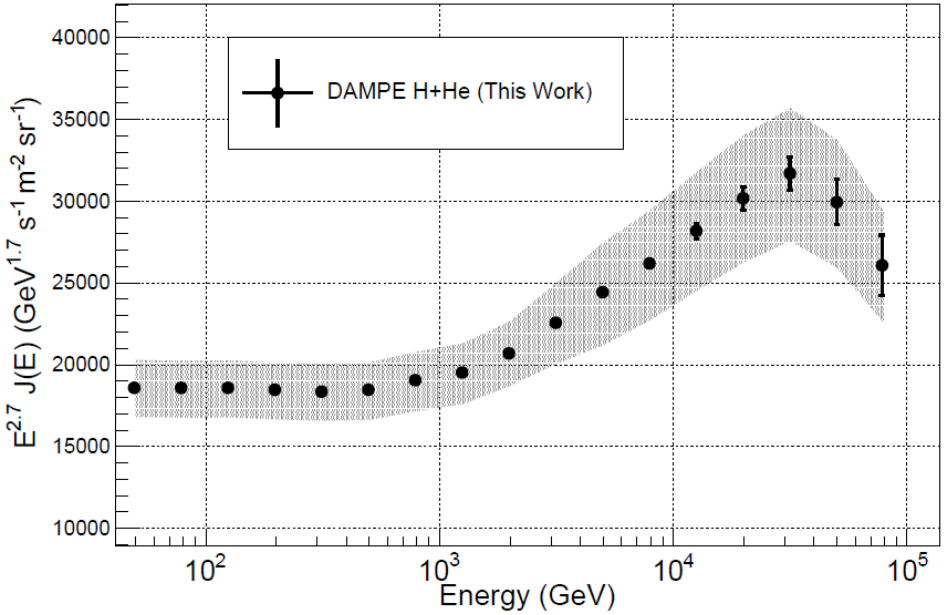

Energy (GeV)	Energy bin interval (GeV)	$\Phi \pm \sigma_{stat} \pm \sigma_{sys}$ (GeV^{-1} s^{-1} m^{-2} sr^{-1})
49.8	39.8-63.1	$(4.77 \pm 0.001 \pm 0.45) \times 10^{-1}$
78.9	63.1-100.0	$(1.37 \pm 0.0005 \pm 0.13) \times 10^{-1}$
125.1	100.0-158.5	$(3.96 \pm 0.002 \pm 0.37) \times 10^{-2}$
198.3	158.5-251.2	$(1.13 \pm 0.0008 \pm 0.11) \times 10^{-2}$
314.2	251.2-398.1	$(3.26 \pm 0.003 \pm 0.31) \times 10^{-3}$
498.1	398.1-630.9	$(9.43 \pm 0.01 \pm 0.90) \times 10^{-4}$
789.5	630.9-1000.0	$(2.81 \pm 0.01 \pm 0.27) \times 10^{-4}$
1251.2	1000.0-1584.9	$(8.30 \pm 0.03 \pm 0.79) \times 10^{-5}$
1983.0	1584.9-2511.9	$(2.54 \pm 0.01 \pm 0.24) \times 10^{-5}$
3142.9	2511.9-3981.1	$(8.00 \pm 0.05 \pm 0.88) \times 10^{-6}$
4981.2	3981.1-6309.6	$(2.50 \pm 0.02 \pm 0.32) \times 10^{-6}$
7894.6	6309.6-10000.0	$(7.70 \pm 0.09 \pm 0.99) \times 10^{-7}$
12512.6	10000.0-15848.9	$(2.40 \pm 0.04 \pm 0.31) \times 10^{-7}$
19830.3	15848.9-25118.9	$(7.4 \pm 0.17 \pm 0.95) \times 10^{-8}$
31429.2	25118.9-39810.7	$(2.24 \pm 0.07 \pm 0.29) \times 10^{-8}$
49812.5	39810.7-63095.7	$(6.10 \pm 0.28 \pm 0.8) \times 10^{-9}$
78946.7	63095.7-100000.0	$(1.53 \pm 0.11 \pm 0.20) \times 10^{-9}$

The DAMPE H + He spectrum shows the spectral hardening at ~500 GeV, moreover, a spectral softening at ~30 TeV can also be observed. This is consistent with the softening observed by DAMPE in the H only spectrum, suggesting a Z dependence of this unexpected feature.

Measurement of the H + He flux

Final spectrum

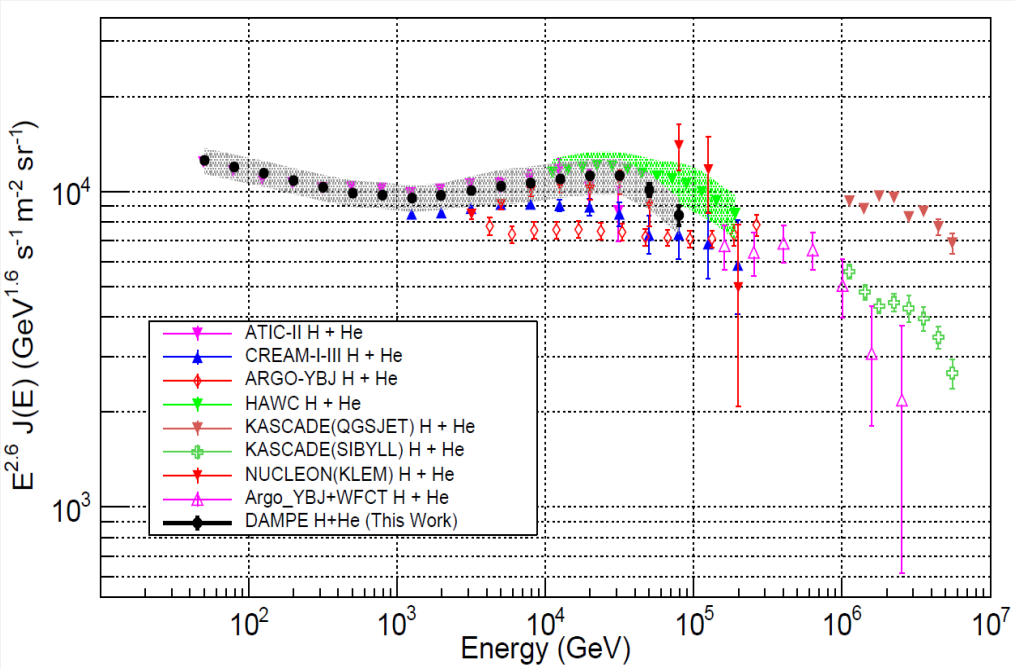

- A precise measurement of H + He spectrum that spans three decades of energy was obtained
- The spectral hardening at ~500 GeV was confirmed, and a spectral softening at ~30 TeV was clearly observed
- Fair agreement with ATIC, NUCLEON, CREAM and HAWC measurements
- The extrapolation of the spectrum up to 1 PeV might be agree with the ARGO-YBJ and KASCADE (SIBYLL) results

PART 05 Summary

Summary

- DAMPE is able to measure CR nuclei up to the energy of hundreds TeV with **unprecedented energy resolution and statistics**

- The difficulties on reconstructing the energy of the hadron shower were discussed. The Bayes method was used to solve these problems. The **reliability of the Bayes method** was tested by both the beam data and MC samples, several hadronic interaction models were also considered

- The data analysis on the H + He spectrum was discussed. **The H + He spectrum with energy from 40 GeV up to 100 TeV was measured**. A spectral hardening was observed at ~ 500 GeV confirming the previous measurements. **Moreover, a spectral softening was found at ~ 30 TeV, pointing out a new feature in the galactic CR flux**

Scientific publications:

- G. Ambrosi et al., Direct detection of a break in the tera electron volt cosmic-ray spectrum of electrons and positrons. ***Nature*, 552 (2017), 63–66**.
- Z. M. Wang et al., Temperature dependence of the plastic scintillator detector for DAMPE. ***Chinese Physics C*, 41 (2017), 016001**.
- Y. Yu et al., The Plastic Scintillator Detector at DAMPE. ***Astroparticle Physics***, **94 (2017)**, **1-10**.
- A. Tykhonov et al., Internal alignment and position resolution of the silicon tracker of DAMPE determined with orbit data. ***Nuclear Instruments and Methods in Physics Research A***, **893 (2017)**, **43-56**.
- H. Zhao et al., A machine learning method to separate electrons from protons from 10 GeV to 100 GeV using DAMPE data**.** ***Research in Astronomy and Astrophysics,*** **18 (2018)**, **6**.
- J. Chang et al., The Dark Matter Particle Explorer mission. ***Astroparticle Physics*, 95 (2018), 6-24.**
- I. De Mitri et al., Measurement of the Cosmic-ray Proton + Helium Spectrum with DAMPE. **PoS(ICRC2019)148 (2019)**.
- Q. An et al., Measurement of the cosmic ray proton spectrum from 40 GeV to 100 TeV with the DAMPE satellite. ***Science Advances***, **5 (2019)**, **eaax3793**.

Conferences/Workshops/Seminars

- 5th HERD workshop, CERN, Switzerland, 11 - 12 October 2017;
- 7th international DAMPE workshop, Nanjing, China, 19 - 21 December 2017 (**Talk Title: Check of proton energy reconstruction using test beam data**);
- Cosmic RAy Transport and Energetic Radiation (CRATER)conference, L'Aquila, Italy, 28, May - 1, June2018;
- 7th HERD workshop, CERN, Switzerland, 6 - 7 November, 2018;
- 8th international DAMPE workshop, L'Aquila, Italy, 10 - 12 December 2018 (**Talk Title: Study on the galactic cosmic ray proton + helium flux**);
- WIN2019. The 27th International Workshop on Weak Interactions and Neutrinos, Bari, Italy, 3 - 8 June 2019 (**Talk Title: DAMPE space mission and recent results**);
- 9th international DAMPE workshop, Lanzhou, China, 15 - 17 June 2019 (**Talk Title: Status of the proton + helium analysis in GSSI**);
- 36th International Cosmic Ray Conference (ICRC), Madison, Wisconsin, USA 24, July – 1, August 2019 (**Poster title: Measurement of cosmic-ray proton + helium spectrum with DAMPE**).

Summer schools

- International School of Space Science, L'Aquila, Italy, 2, July - 8, July;
- XXX International Seminar of nuclear and sub-nuclear physics "Francesco Romano", Otranto, Italy, 5 - 12 June 2018 (**Talk Title: DAMPE space mission and recent results**);
- International School for Astroparticle Physics, LHC meets Cosmic Rays, CERN, Switzerland, 28 October – 2 November 2018.

Awards

- Best student presentation award in "XXX International Seminar of nuclear and sub-nuclear physics 'Francesco Romano'", 2018

Outreach activities

- 6th Astroparticle Physics Science Fair at GSSI, L'Aquila, 2020
- The International Cosmic Day, LNGS, 2019
- 5th Astroparticle Physics Science Fair at GSSI, L'Aquila, 2019

THANK YOU!

BACK-UP

PART 02

Trigger types of DAMPE

UnBiased Trigger (UBT): each red bar in the first two layers has the signals larger than 0.4 MIPs;

Minimum Ionizing Particle Trigger (MIPT): each red bar has the signals larger than 0.4 MIPs in the first two plus penultimate two (or the second two plus last two) layers of the BGO;

Low Energy Trigger (LET) : requires a threshold of 0.4 MIPs in the first two layers and of 2 MIPs in the second two layers of the BGO;

High Energy Trigger (HET): each red bar has a signal larger than 10 MIPs in the rst three layers and larger than 2 MIPs in the fourth layer of the BGO

The UBT, MIPT and LET are pre-scaled with ratios of 512:1, 4:1 and 8:1 respectively, when the satellite is within the geographical latitude [-20, 20]. For the other parts of the latitude, the UBT and LET are pre-scaled with ratio of 2048:1 and 64:1 respectively, and the MIPT is disabled. HET is not pre-scaled.
The four types of trigger follow the OR-ed logic to decide a global trigger.

PART 04

Dead time : SAA

The South Atlantic Anomaly (SAA), an area with reduced magnetic intensity, where the inner radiation belts (Van Allen belts) come close to the surface of the Earth. This leads to the fluxes of protons and electrons (with energies lower than 100 MeV mainly) captured by the geomagnetic field being two times higher than the fluxes outside of this region. DAMPE will cross SAA six or seven times per day, the data collected there will be eliminated. In total, this part accounts for 4.5% of the total time.

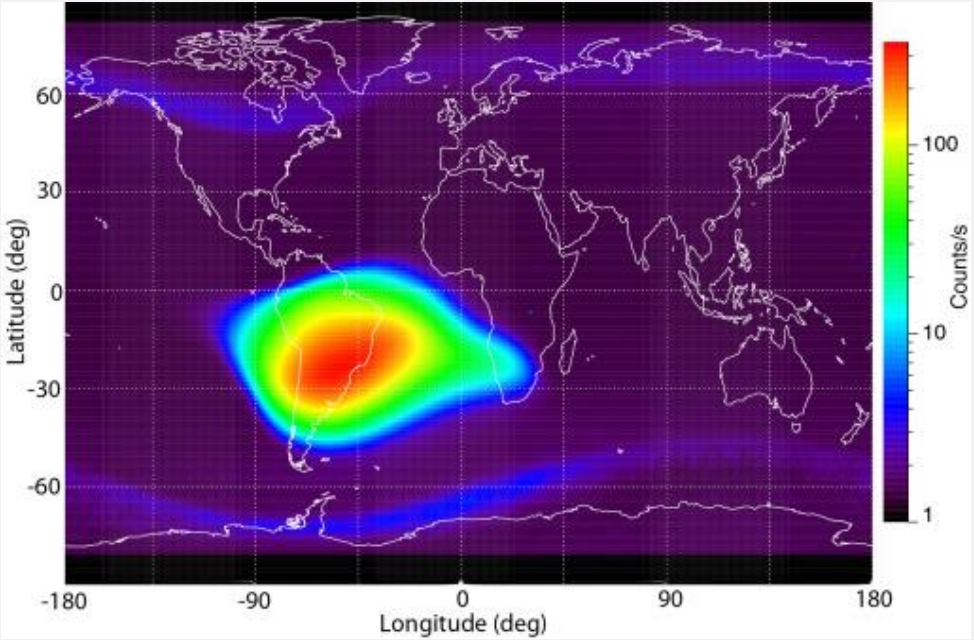

PART 04

Dead time : response time

The response time of DAMPE electronics. When DAMPE is under the normal observation mode, the data acquisition system needs 3.0725 ms for each entering particle to finish the work of reading and storing their signals and recovering the electronics of the detector unit to prepare for next collection. During this period, the trigger system will be vetoed with no response to upcoming particles. Since the general trigger rate of DAMPE is around 70 Hz, the corresponding dead time accounts for 18% of the total time.

PART 04

Dead time : detector Calibration

The on-orbit calibration. An on-orbit calibration of each sub-detector is performed every day in order to guarantee a high quality of the measurement . The calibration includes:

- The STK baseline calibration (30 times per day, each of them lasts 40 s);
- The PSD, BGO and NUD baseline calibrations (once per day, each lasts 100 s);
- Electronics linearity for every sub-detector (once per month, each lasts 30 mins);

The dead time due to the calibrations accounts for 1.8% of the total time.

PART 04

Pre-selection:

- The deposited energy in the BGO has to be larger than 20 GeV. This selection avoids the H + He candidates to be affected by the geomagnetic rigidity cutoff effectively;
- The reconstructed track by the BGO must be fully contained in the calorimeter, i.e., to be inside [-280mm, 280mm] in x-axis and y-axis, and inside [46mm, 448mm] in z-axis of the DAMPE coordinate system. Setting this constraint on the span of the BGO track ensures the shower of the event being well-contained and removes events entering BGO from the detector side;
- The largest energy deposition in a single layer of the BGO should be less than 35% of its total energy deposition. This is to enhance the rejection power for side-incident particles;
- For the top three layers of the BGO, the bar with the largest energy deposition must not be the edge bar of that layer. This cut avoids particle showers being initialized at corner of the BGO.

PART 04

Track selection:

- The track is reconstructed with χ^2 /*ndof* lower than 25 to ensure the reconstruction quality;
- The track must have at least one cluster in X or Y layer of the rst STK plane to ensure an additional charge measurement;
- The angle between the STK track and BGO track must be less than 25° ;
- The distance between projections of the STK and BGO tracks on first layer of BGO must be less than 60 mm (for both XZ and YZ view);
- The distance between projections of BGO and STK tracks on the rst layer of the STK must be less than 200 mm (for both XZ and YZ views);
- STK track-ID match;

PART 04

Track selection:

- The track is reconstructed with χ^2 /*ndof* lower than 25 to ensure the reconstruction quality;
- The distance between projection of the best track and the position of BGO bar with maximum energy deposition must be less than 30 mm on first layer of the BGO;
- The projection of the best track on first layer of the PSD has to be within [-400mm, 400mm] for both XZ and YZ view in DAMPE coordinate system to ensure the track passing through the PSD;
- The PSD bars traversed by the track must have energy depositions higher than 0.5 MeV in order to make possible the reconstruction of particle charge.

PART 04

Removal of electron and positron particles

A variable ζ is defined as:

$$\zeta = \mathcal{F} \cdot \frac{(\sum_{i=0}^{13} RMS_i)^4}{8000000}$$

with:

$$RMS_i = \sum_{j=0}^{21} (xj_{,i} - x_{c,i})^2 \cdot E_{j,i}$$

- $\mathcal{F}$: the ratio between the energy deposition in the last BGO layer over the total energy deposition;
- $x_{j,i}$: the coordinate of j-th bar in i-th layer of the BGO;
- $E_{j,i}$: deposited energy in the same bar;
- $x_{c,i}$: the coordinate of j-th bar in i-th layer of the BGO.

PART 04

Removal of electron and positron particles

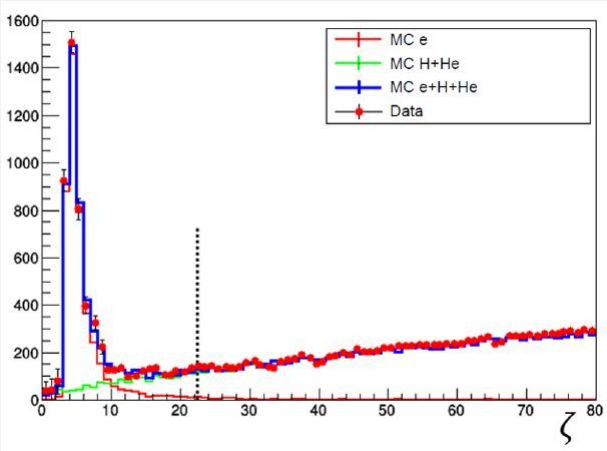

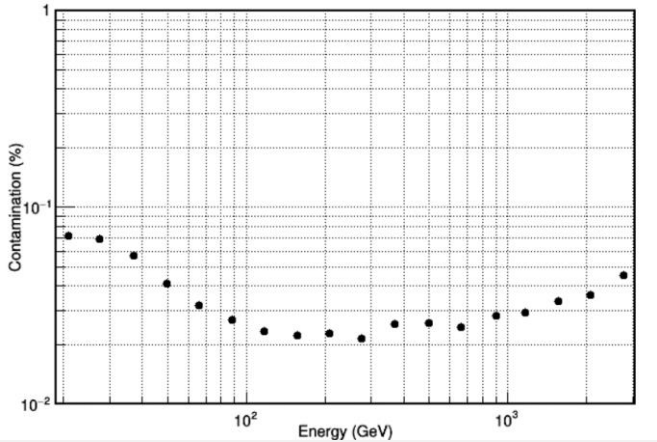

By using of $\mathcal{F}$ and RMS, the hadron and lepton particles can be well estimated. The contamination is within 0.1%, which is negligible compared with other systematic uncertainties.

PART 04

Charge selection

The charge selection is based on the variable ΔE_{track} , which is defined as:

$$\Delta E_{track} = (E_1 + \mathrm{E}_2) \cdot 10/(L_1 + L_2)$$

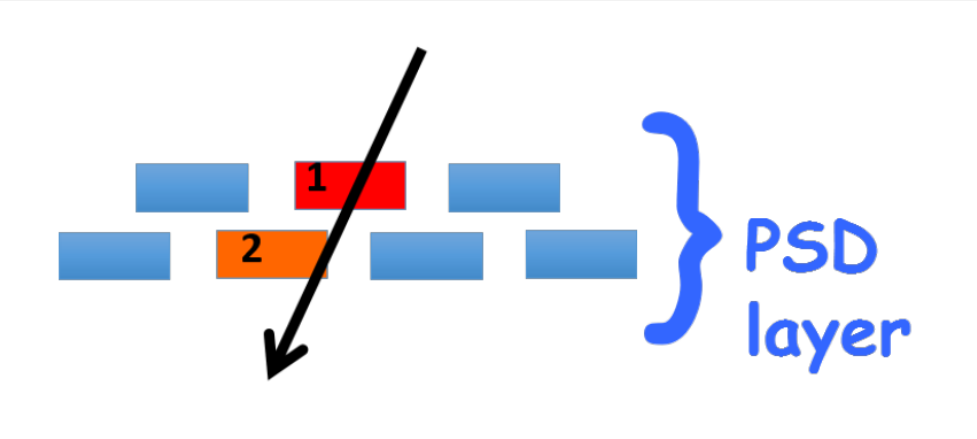

$\Delta Etrac_k$ combines the two PSD sub-layer measurements and corrects the incident angle at the same time.

PART 04

Charge selection

Since there are two PSD layers, each of them can give an independent measurement ($\Delta Etrac_{kX}$ and $\Delta Etrac_{kY}$), we will use the variable E_{PSD} , which equals $(\Delta Etrac_{kX} + \Delta Etrac_{kY})/2$ to perform the charge selection.

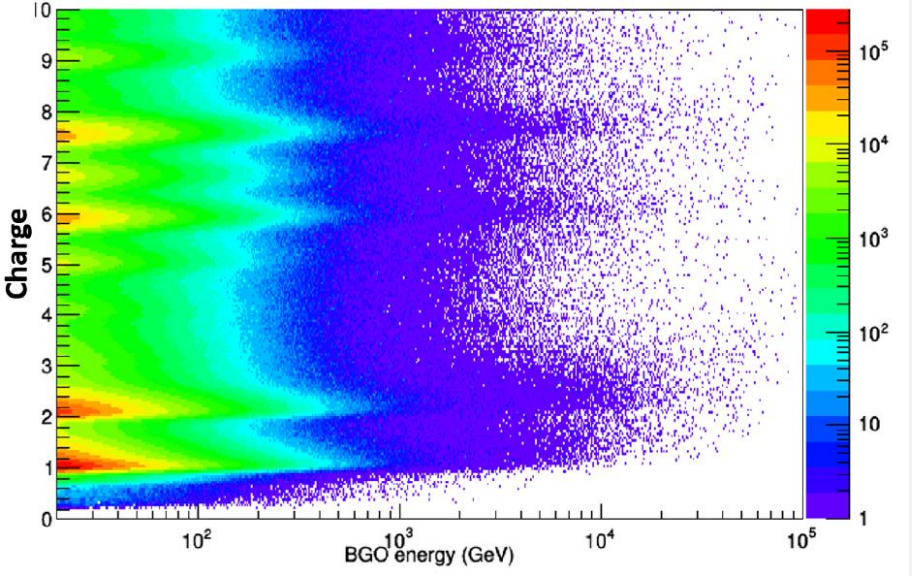

The reconstructed charge based on E_{PSD}

PART 04

Energy reconstruction

The initial energy of H + He candidates need to be reconstructed by using the Bayes method discussed in part 3.

$$N(E_T^i)=\sum_{j=1}^{n} P(E_T^i|E_{BGO}^j)\cdot N\left(E_{BGO}^j\right), j=1,2,\ldots$$

$N\left(E_T^i\right)$: The event number of the candidates in i-th bin of the reconstructed energy;

$N\left(E_{BGO}^i\right)$: The event number of the candidates in j-th bin of the BGO energy;

$P(E_T^i|E_{BGO}^j)$: The unfolding matrix.

PART 04

Energy reconstruction

$P(E_T^i|E_{BGO}^j)$ can be derived through Bayes theorem:

$$P(E_T^i|E_{BGO}^j)=\frac{P\left(E_{BGO}^j\middle|E_T^i\right)P_0(E_T^i)}{\sum_{i=1}^{n}P\left(E_{BGO}^j\middle|E_T^i\right)P_0(E_T^i)}$$

$P\left(E_{BGO}^j\middle|E_T^i\right)$: The response matrix, which represents the probability for a particle with energy of E_T^ibeing observed with energy E_{BGO}^j in the BGO calorimeter, which can be obtained with MC simulation.

$P_0(E_T^i)$: The marginal probability, which can be decided from the previous experiments, and updated during the iteration of the unfolding procedures.

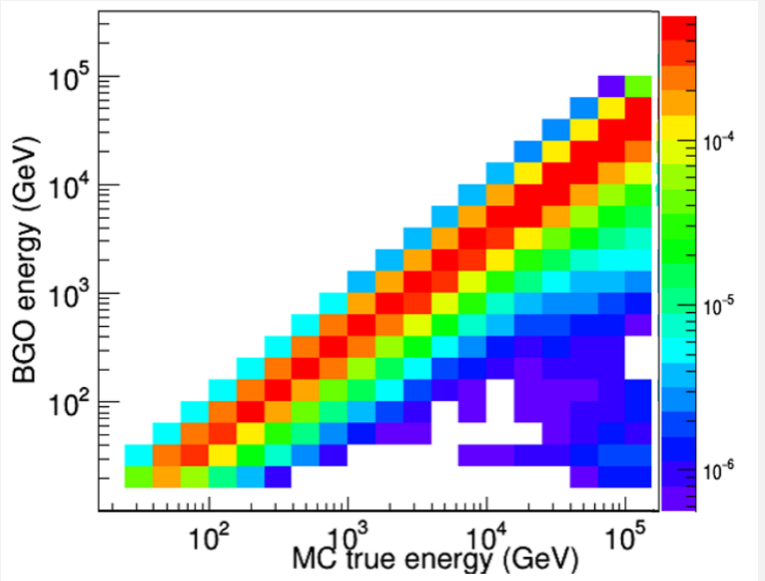

$P\left(E_{BGO}^j\middle|E_T^i\right)$ used in this analysis

PART 04

Unfolding iteration terminating condition

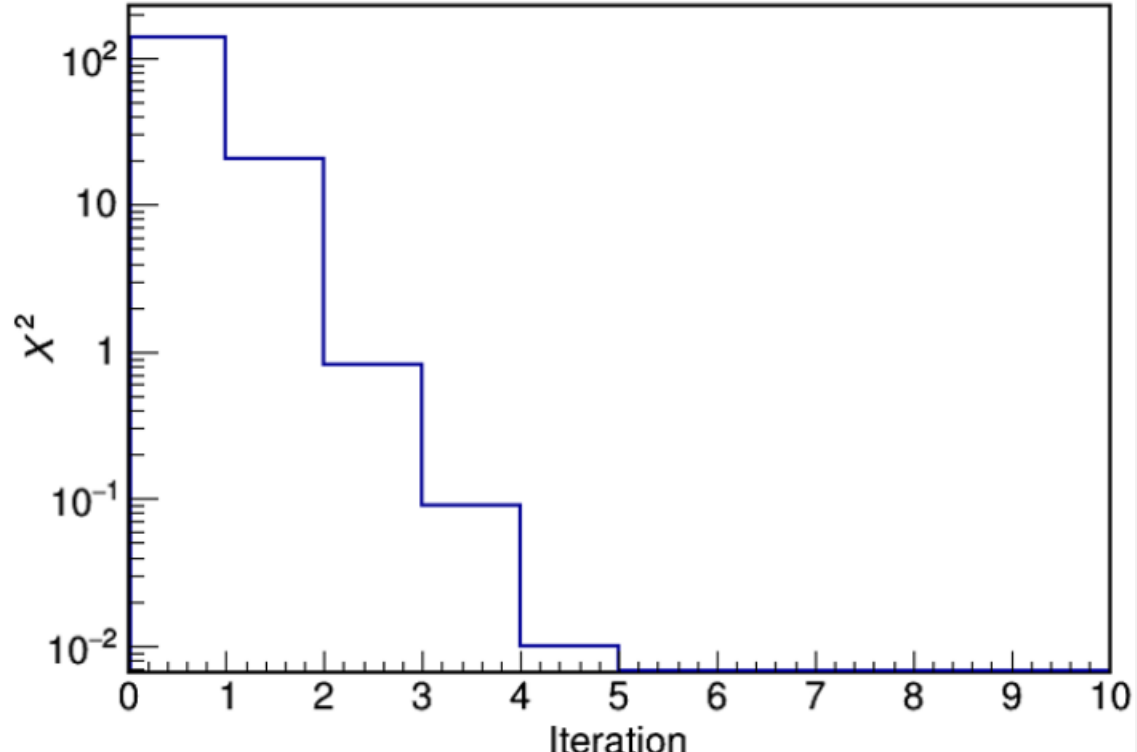

$$\chi^2 = \sum_{j}^{n} \left(\frac{\hat{N}^{j}_{Af} - \hat{N}^{j}_{Bef}}{\sqrt{\hat{N}^{j}_{Bef}}} \right)^2$$

PART 04

Energy reconstruction

Effect of the energy unfolding on the energy distribution of the candidates

Energy bin (GeV)	Events before the unfolding	Events after the unfolding
25.1-39.8	24998978	3813946
39.8-63.1	7372579	12962485
63.1-100.0	3637847	9892676
100.0-158.5	172219	5518425
158.5-251.2	800674	2825416
251.2-398.1	372859	1372626
398.1-630.9	174554	665092
630.9-1000.0	83852	324701
1000.0-1584.9	41191	157393
1584.9-2511.9	20429	79340
2511.9-3981.1	10100	40879
3981.1-6309.6	5037	20853
6309.6-10000.0	2588	10691
10000.0-15848.9	1273	5483
15848.9-25118.9	535	2807
25118.9-39810.7	212	1395
39810.7-63095.7	134	626
63095.7-100000.0	27	254

$$\Phi(E, E+\Delta E) = \frac{N_{\mathrm{H+He}}(E, E+\Delta E)}{\Delta T \cdot A_{acc} \cdot \Delta E}$$

All the components are derived, the flux can be calculated!

PART 04

High Energy Trigger efficiency of QGSP simulation:

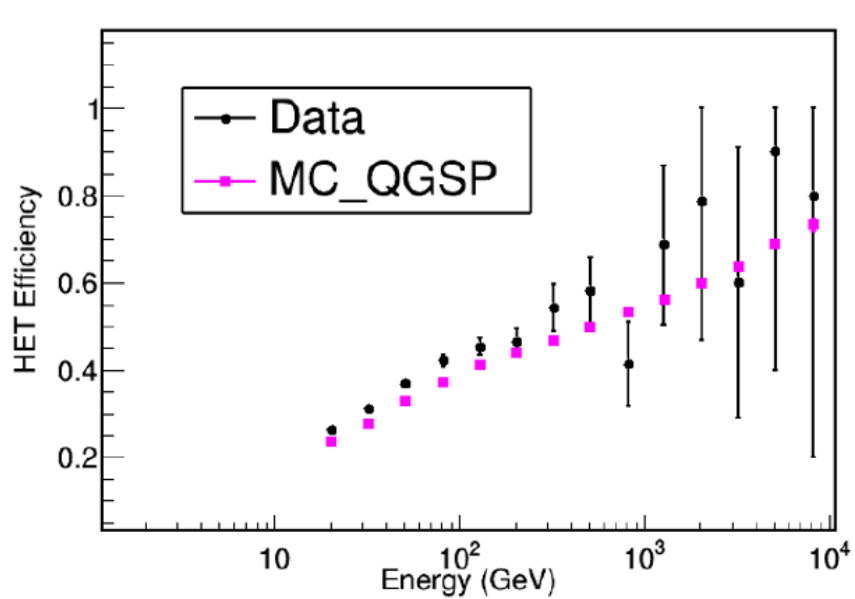

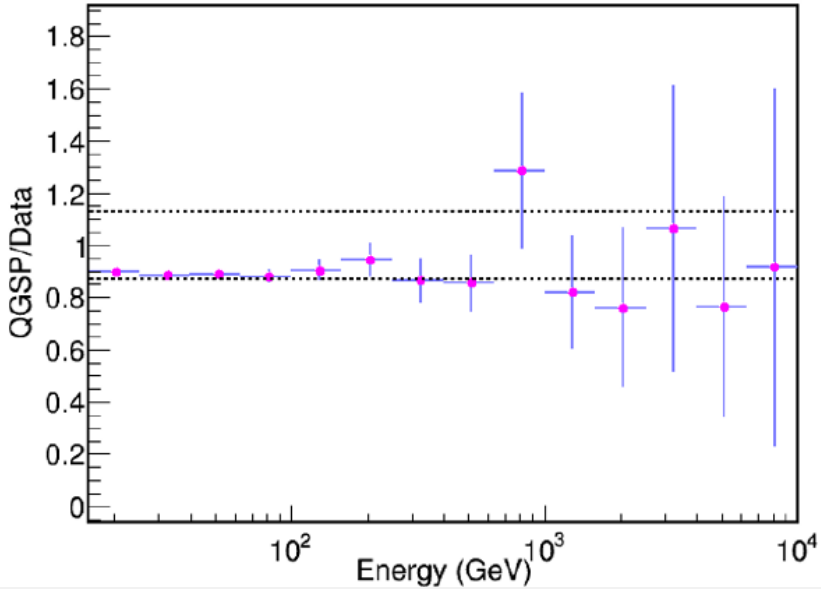

The difference is within 13%

PART 04

PSD correction

$$E_{\mathrm{PSD-cor}}=(E_{\mathrm{PSD}}-f_{\mathrm{MCMPV}}(E_{\mathrm{BGO}}))\cdot\frac{f_{\mathrm{dataSigma}}(E_{\mathrm{BGO}})}{f_{\mathrm{MCSigma}}(E_{\mathrm{BGO}})}+f_{\mathrm{dataMPV}}(E_{\mathrm{BGO}})$$

$E_{\mathrm{PSD-cor}}$: E_{PSD} after the correction;
$f_{\mathrm{MCMPV}}(E_{\mathrm{BGO}})$: MPV of the MC fitting functions;
$f_{\mathrm{dataMPV}}(E_{\mathrm{BGO}})$: MPV of the orbit data fitting functions;
$f_{\mathrm{MCSigma}}(E_{\mathrm{BGO}})$: Sigma of the MC fitting functions;
$f_{\mathrm{dataSigma}}(E_{\mathrm{BGO}})$: Sigma of the data fitting functions.

The equation correct both the MPV and the sigma of the distribution.

PART 04

Contamination from electron and heavy nuclei

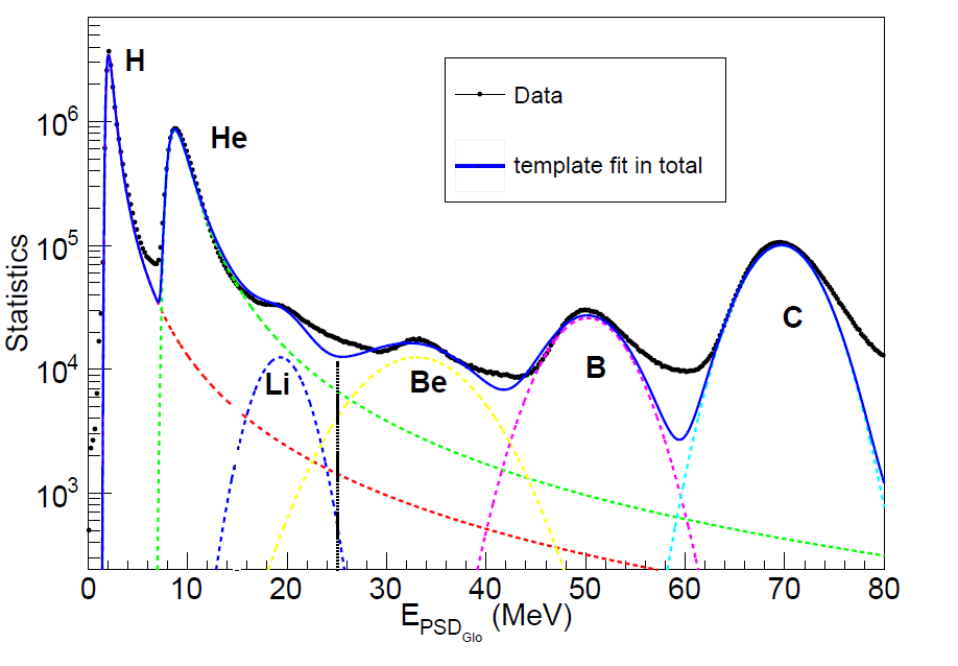

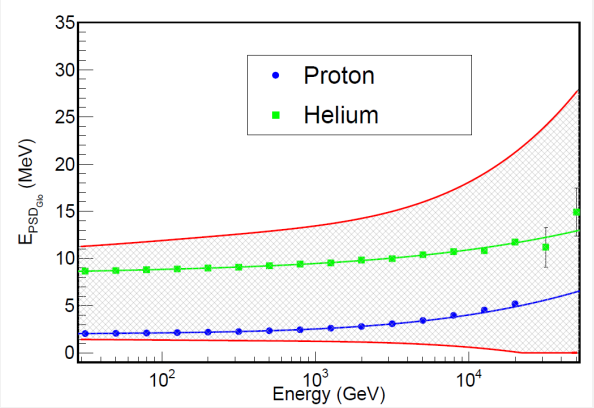

Element	Li	Be	B	C	Total
Contamination	0.71%	0.019%	—	—	0.73%

The contamination is less than 1%, which is also negligible.

PART 04

Charge reconstruction efficiency without the PSD correction:

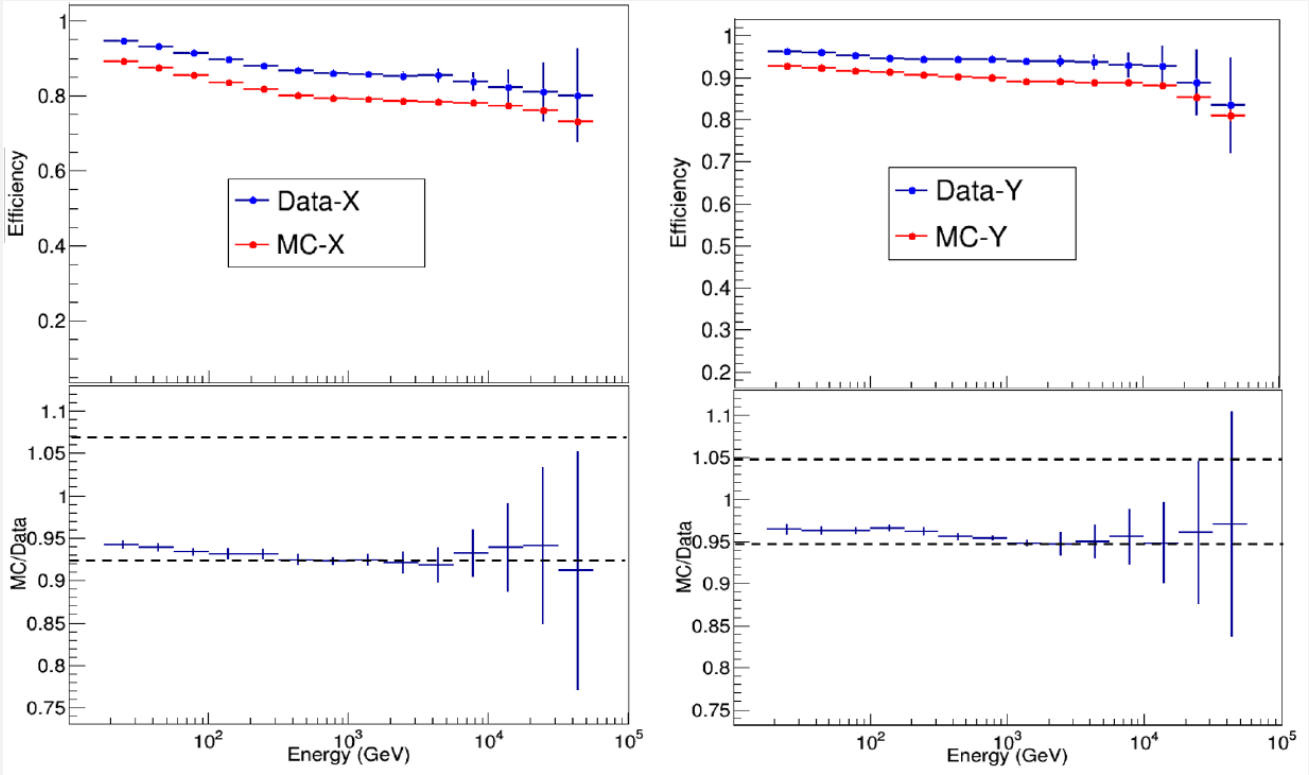

The difference is within 7%, which is larger than the situation with the PSD correction.

PART 04

Geometric factor correction

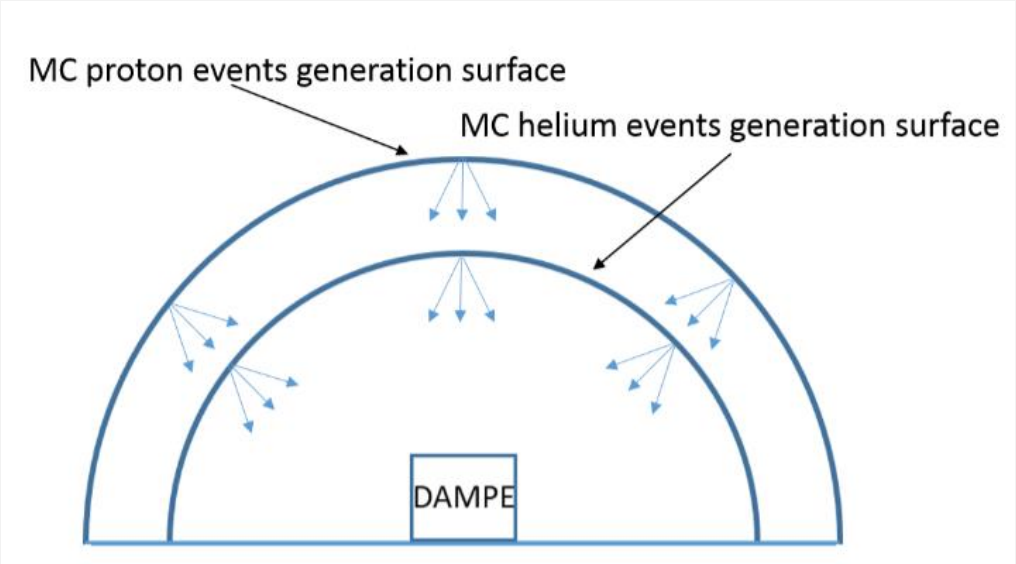

$$A_{acc_{He}} = \frac{N_{sel_{He}}}{N_{gen_{He}}} \cdot \varsigma_H \cdot \frac{\varsigma_{He}}{\varsigma_H}$$

$$A_{acc_{H+He}} = \frac{N_{sel_H} + N_{sel_{He}} \cdot (\varsigma_{He}/\varsigma_H)}{N_{gen_H} + N_{gen_{He}}} \cdot \varsigma_H \cdot$$

PART 04

Geometric factor correction

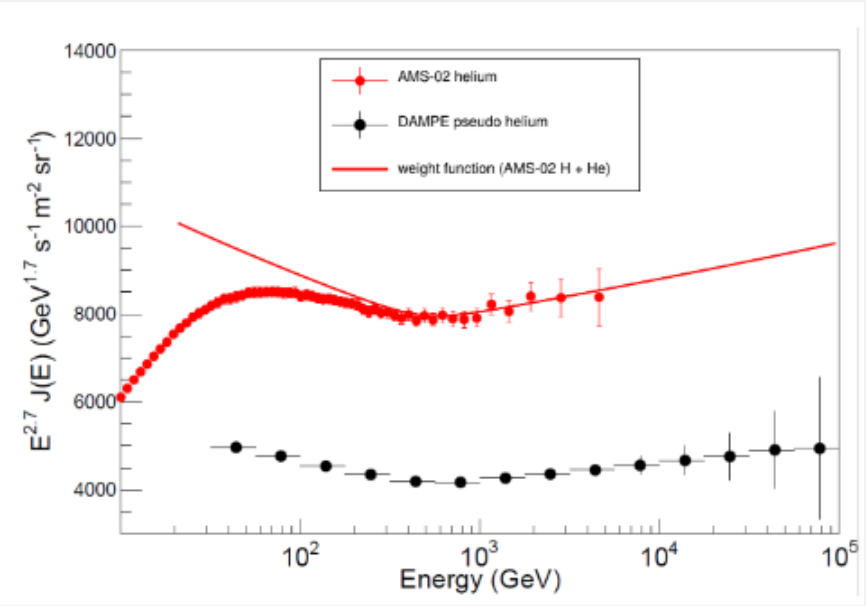

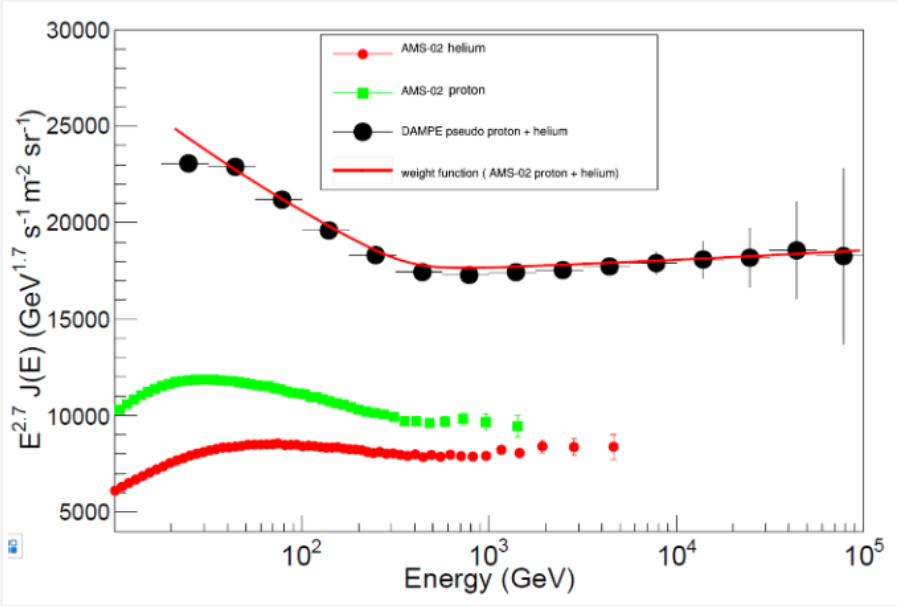

PART 04

Energy scale

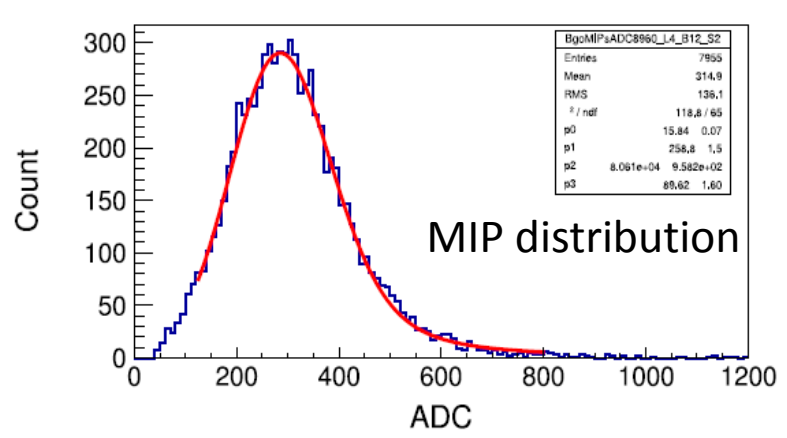

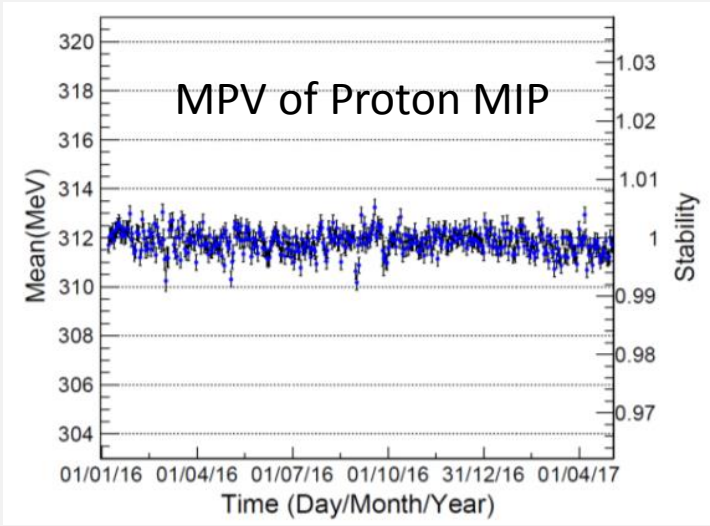

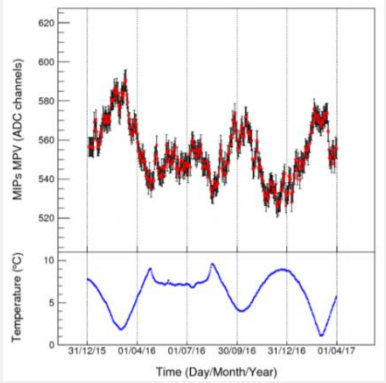

After temperature correction and attenuation correction, the stability of energy measurement is better than 1%.